IR 78-1589

REPORT NO. DOT/MTB/OHMR-78-4

Analysis of the Pneumatic Burst of a Large Seamless Steel Pressure Vessel in Natural Gas Service

by

Bruce W. Christ
Fracture and Deformation Division
Center for Materials Science
National Bureau of Standards
U.S. Department of Commerce
Washington, D.C. 20234

December, 1978

Final Report

Issued March 1979

Document is available to the U.S. public through
the National Technical Information Service,
Springfield, Virginia 22161

Prepared for

U.S. DEPARTMENT OF TRANSPORTATION
MATERIALS TRANSPORTATION BUREAU
Office of Hazardous Materials Regulations
Washington, D.C. 20590

NOTICE

The contents of this report reflect the views of the author who is responsible for the facts and the accuracy of the data presented herein. The contents do not necessarily reflect the official views or policy of the Department of Transportation. This report does not constitute a standard, specification or regulation.

This document is disseminated under the sponsorship of the Department of Transportation in the interest of information exchange. The United States Government assumes no liability for its contents or use thereof.

NBSIR 78-1589

ANALYSIS OF THE PNEUMATIC BURST OF A LARGE SEAMLESS STEEL PRESSURE VESSEL IN NATURAL GAS SERVICE

Bruce W. Christ

Fracture and Deformation Division
Center for Materials Science
National Measurements Laboratory
National Bureau of Standards
U.S. Department of Commerce
Washington, D.C. 20234

Failure Analysis Report

December, 1978

Issued March 1979

Prepared for
Office of Hazardous Materials Regulations
Materials Transportation Bureau
Department of Transportation
Washington, D.C. 20590

Contract No. DOT AS-40034

NOTICE

The contents of this report reflect the views of the author who is responsible for the facts and the accuracy of the data presented herein. The contents do not necessarily reflect the official views or policy of the Department of Transportation. This report does not constitute a standard, specification or regulation.

This document is disseminated under the sponsorship of the Department of Transportation in the interest of information exchange. The United States Government assumes no liability for its contents or use thereof.

Technical Report Documentation Page

1. Report No.	2. Government Accession No.	3. Recipient's Catalog No.
DOT/RSPA/MTB-78/4		

4. Title and Subtitle	5. Report Date
Analysis of the Pneumatic Burst of a Large Seamless Steel Pressure Vessel in Natural Gas Service	March 1979
	6. Performing Organization Code
7. Author(s)	8. Performing Organization Report No.
Bruce W. Christ	NBSIR 78-1589
9. Performing Organization Name and Address	10. Work Unit No. (TRAIS)
Fracture and Deformation Division National Bureau of Standards Washington, DC 20234	11. Contract or Grant No. DOT AS 40034
	13. Type of Report and Period Covered
12. Sponsoring Agency Name and Address	
Office of Hazardous Materials Regulation Materials Transportation Bureau U.S. Department of Transportation Washington, DC 20590	14. Sponsoring Agency Code DOT/MTB/OHMR

15. Supplementary Notes

16. Abstract At the request of the Office of Hazardous Materials Regulation (OHMR) - U.S. Department of Transportation (DOT), the NBS Fracture and Deformation Division carried out a metallurgical evaluation and fracture analysis of a pneumatically-burst seamless steel compressed gas cylinder which was used for over-the-highway transport of natural gas. The relevant specification for this pressure vessel is Specification DOT 3T. The cylinder was 34-feet long by 22-inches diameter, with a wall thickness of about 1/2-inch. It was new and had been in service for about a week. The cylinder burst during filling. Reported burst pressure was believed to be 2,200 to 2,500 psi. Expected burst pressure was 6,800 psi. Tensile strength of this quenched and tempered low alloy steel pressure vessel (0.44 carbon - 0.92 manganese - 0.98 chromium - 0.20 molybdenum) ranged between 136,200 and 170,500 psi. The cylinder ruptured due to environmentally-assisted cracking. The fracture originated at a part-through crack in a region of high tensile strength. At the time of rupture, the fracture origin was about 1.3-inches long and penetrated half the wall thickness from the inside. Four other part-through cracks were found in the vicinity of the fracture origin. They were linked to tiny circumferential cracks (blister cracks) in rather hard microzones (HRC 40 to 45) within about 0.01-inches of the inside wall. Up to 500 ppm by volume of hydrogen sulfide was detected in gas samples taken from the natural gas wells after the incident. Evidence of sulfur was found on the fracture origin and on the inside wall. It was concluded that the rupture was due to the internal gas pressure acting on the region of the fracture origin. It is probable that the fracture origin and the other part-through cracks developed from service stresses acting on blister cracks. The blister cracks probably formed as diffusible hydrogen (cont'd)

17. Key Words	18. Distribution Statement
Pressure vessel, Pneumatic rupture, Natural gas, Steel, Hydrogen sulfide, DOT Specification 3T, Stress corrosion	This document is available to the U.S. public through the National Technical Information Service, Springfield, Virginia 22161

19. Security Classif. (of this report)	20. Security Classif. (of this page)	21. No. of Pages	22. Price
Unclassified	Unclassified	120	$6.50

Form DOT F 1700.7 (8-72) Reproduction of completed page authorized

Technical Report Documentation Page

DOT/RSPA/MTB-78/4 Analysis of the Pneumatic Burst of a Large Seamless Steel Pressure Vessel in Natural Gas Service

By: Bruce W. Christ
Fracture and Deformation Division
National Bureau of Standards
Washington, DC 20234

16. Abstract (cont'd)

from the decomposition of hydrogen sulfide interacted with the hard microzones close to the inside wall. It is likely that the rupture occurred in such a short time due to the combination of high hydrogen sulfide concentration in the natural gas and rather high-hardness microzones in the steel near the inside wall.

ANALYSIS OF THE PNEUMATIC BURST OF A LARGE SEAMLESS STEEL PRESSURE VESSEL IN NATURAL GAS SERVICE

by

Bruce W. Christ

Fracture and Deformation Division
National Bureau of Standards
Washington, DC 20234

TABLE OF CONTENTS

TABLE OF CONTENTS (continued)

ANALYSIS OF THE PNEUMATIC RUPTURE OF A LARGE PRESSURE VESSEL IN NATURAL GAS SERVICE

ABSTRACT

At the request of the Office of Hazardous Materials Regulation (OHMR) - U.S. Department of Transportation (DOT), the NBS Fracture and Deformation Division carried out a metallurgical evaluation and fracture analysis of a pneumatically-burst seamless steel compressed gas cylinder which was used for over-the-highway transport of natural gas. The relevant specification for this pressure vessel is Specification DOT 3T. The cylinder was 34-feet long by 22-inches diameter, with a wall thickness of about 1/2-inch. It was new and had been in service for about a week. The cylinder burst during filling. Reported burst pressure was believed to be 2,200 to 2,500 psi. Expected burst pressure was 6,800 psi. Tensile strength of this quenched and tempered low alloy steel pressure vessel (0.44 carbon - 0.92 manganese - 0.98 chromium - 0.20 molybdenum) ranged between 136,200 and 170,500 psi. The cylinder ruptured due to environmentally-assisted cracking. The fracture originated at a part-through crack in a region of high tensile strength. At the time of rupture, the fracture origin was about 1.3-inches long and penetrated half the wall thickness from the inside. Four other part-through cracks were found in the vicinity of the fracture origin. They were linked to tiny circumferential cracks (blister cracks) in rather hard microzones (HRC 40 to 45) within about 0.01-inches of the inside wall. Up to 500 ppm by volume of hydrogen sulfide was detected in gas samples taken from the natural gas wells after the incident. Evidence of sulfur was found on the fracture origin and on the inside wall. It was concluded that the rupture was due to the internal gas pressure acting on the region of the fracture origin. It is probable that the fracture origin and the other part-through cracks developed from service stresses acting on blister cracks. The blister cracks probably formed as diffusible hydrogen from the decomposition of hydrogen sulfide interacted with the hard microzones close to the inside wall. It is likely that the rupture occurred in such a short time due to the combination of high hydrogen sulfide concentration in the natural gas and rather high-hardness microzones in the steel near the inside wall.

1. GENERAL INFORMATION

1.1 Reference

U.S. Department of Transportation, Materials Transportation Bureau, Office of Hazardous Materials Regulation, Engineering Branch, 2100 - 2 nd Street, S.W., Washington, DC 20590. This report was prepared at the request of Mr. Arthur J. Mallen, Engineering Branch Chief, in a letter dated January 5, 1979. Contract DOT AS-40034 supported this work.

1.2 Background

The information in the following four paragraphs was provided by Mr. A. J. Mallen.

On October 27, 1977 at about 6:30 p.m., a seamless steel compressed gas cylinder burst while it was being filled with natural gas at the wellhead. The incident occurred near Litchfield, Kentucky in an isolated rural setting.

The DOT Serial Number stamped on the burst cylinder was 9959. The burst cylinder was new. It had been manufactured in July, 1977. The history of the cylinder between July and October was not recorded.

The cylinder was one of twelve cylinders mounted in fixed positions on a "tube trailer" used for transporting compressed gases over the public highways. The trailer permit was issued by the Kentucky State Fire Marshal's Office on October 6, 1977. The relevant specification for manufacture of the cylinder was Department of Transportation Specification 3T, appearing in Part 178, Subpart C, Section 178.45 of the Code of Federal Regulations, Title 49.[1] Mr. Arthur Mallen supplied NBS with

copies of the test reports[2] prepared by the independent inspector approved by the Department of Transportation to carry out inspections and testing during manufacture. The revised test report was dated July 25, 1977. The initial report was dated July 6, 1977.

Following the incident, DOT-OHMR issued rule making to amend the regulations to incorporate a definition of methane, because of evidence that the regulations were not being applied as intended. This amendment emphasized that whereas the regulations (Code of Federal Regulations - Title 49 - Subparagraph 173.302-(a)(3)) authorize shipment of methane in DOT specification cylinders 3AX, 3AAX and 3T, the regulations do not authorize shipment of natural gas.

The further information reported in this section was gathered by B. W. Christ from a number of individuals who were involved with the incident. Some were on the scene shortly after the incident occurred. Others participated in the clean-up during the following weeks. These individuals are listed below.

Mr. Gilbert Ellis
Assistant State Fire Marshal
Frankfort, Kentucky

Mr. William Piehl
Western Sales and Testing
Amarillo, Texas

Mr. Rodney Raby
Deputy State Fire Marshal
Frankfort, Kentucky

Mr. Maurice Bolinger, Jr.
Gladstone Laboratories
Cincinnati, Ohio

Mr. Gobel Mattingly
Compressed Gas Corporation
Litchfield, Kentucky

Mr. Roger McCombs
Gladstone Laboratories
Cincinnati, Ohio

The trailer containing the cylinder which ruptured was identified as trailer number T-256. It was standing on a gravel pad and was being filled via a pipe connection to a large compressor which was pumping natural gas from two wells located about two miles away. Well pressure was about 400 psi, which was the pressure carrying gas to the compressor through the gathering lines. All twelve cylinders on the

trailer were connected via a common manifold. A second trailer, identified as trailer number T-254, was standing on the gravel pad alongside the first. It was awaiting filling.

The charging pressure when the burst occurred was believed to be 2,200 to 2,500 psi. Minimum expected burst pressure was 6,800 psi.* The large difference in pressures suggests the presence of a discontinuity somewhere in the cylinder.

Eleven large pieces formed as a result of the burst. Pieces were flung from 200 to 2,000 feet. Besides the burst cylinder, six others came off trailer T-256. Each remained intact, except for the manifolding. One cylinder landed beneath trailer T-254. Ingition of the natural gas occurred at some time during the incident. Flow of the natural gas was shut off at the compressor shortly after the burst. However, the eleven cylinders from trailer T-256 continued jetting natural gas, which was burning in some cases.

---

*Specification DOT 3T[1] does not contain an explicit statement about design burst pressure. However, a minimum burst pressure for a DOT specification 3T cylinder can be estimated by substituting the minimum allowed tensile strength, 135,000 psi according to Section 178.45-7, into the Bach-Clavarino formula for wall stress found in Subparagraph 178.45-7(b),

$$S = \frac{P(1.3D^2 + 0.4d^2)}{D^2 - d^2}$$

where S = wall stress (hoop stress) in psi = 135,000 psi
P_{min} = gas pressure in psi at burst
D = outside diameter in inches (assumed to be 22 inches)
d = inside diameter in inches (assumed to be 21.06 inches)
t = wall thickness in inches = $\frac{D-d}{2} = \frac{22-21.06}{2} = 0.470$ inches

This estimate is only approximate because the Bach-Clavarino formula is derived from elastic, not plastic, analysis.

$$P_{min} = \frac{S(D^2-d^2)}{1.3D^2 + 0.4d^2} = \frac{135,000\ (22^2-21.06^2)}{1.3\ (22)^2 + 0.4\ (21.06)^2} = 6,800 \text{ psi}$$

The value of P_{min} will vary slightly from cylinder to cylinder, depending on exact diameter and wall thickness.

Each cylinder was equipped with rupture disks, in accord with the regulations. A disk was installed in each end of each cylinder and was set to operate at a pressure of about 3,800 psi. Most of the rupture disks were recovered after the incident. None of those recovered had ruptured. Testing of the recovered disks[3] verified that their operating pressure was about 3,800 psi.

A diagram showing the incident site afterwards appears in Figure 1. The layout of the site itself was traced from a surveyor's diagram provided to NBS by the Kentucky State Fire Marshal's Office. The positions of the pieces of the burst cylinder were noted by Mr. Rodney Raby* of that office. The location of two pieces, RR-18 and RR-19 was not established.

Clean up of the incident site was not immediate. Pieces of the burst cylinder lay where they landed in cornfields for about a week. Eventually, all pieces were dragged to the gravel pad, then loaded on a truck and taken to a bonded warehouse in Louisville, Kentucky.

The weight of the eleven pieces trucked to Louisville on November 4, 1977 was 3694 pounds, as compared to the test-report[2] tare weight for the as-manufactured cylinder of 3642 pounds. This tare weight appears in the revised test report dated July 25, 1977. The difference may be attributed in part to slight inaccuracy in the weighing and/or adhering soil, which was conspicuously evident.

On December 28, 1977, the eleven pieces were trucked to the Gladstone Laboratories in Cincinnati, Ohio for inspection and analysis. Following a request by Mr. Arthur Mallen, Dr. Bruce W. Christ of NBS visited Gladstone Laboratories on January 5, 1978 to provide direction and

---

*Mr. Rodney Raby participated in the recovery of the eleven pieces. His initials are the source of the "RR" designation.

assistance in their investigation. Eventually a cooperative investigative effort developed between NBS and the Gladstone Laboratories.

By March, 1978, material from cylinder 9959 and from two other cylinders was being transmitted to NBS for metallographic and fractographic examination, mechanical properties measurements and chemical analysis. Seven preliminary NBS memo reports related to the burst of cylinder 9959 were submitted to the Office of Hazardous Materials Regulation between January 5, 1978 and July 19, 1978.[4]

Also in March, 1978, Battelle Memorial Institute of Columbus, Ohio began looking into the feasibility of shipping natural gas from the wellhead in DOT 3T specification trailer tubes for Goodyear Corporation, Akron, Ohio. Mr. William Maxey surveyed the eleven pieces of the burst tube 9959 at the Gladstone Laboratories and obtained some material for metallographic and fractographic examination and for mechanical properties testing. Information was exchanged freely between NBS and Battelle. A report on the Battelle findings was issued.[5]

1.3 Identification and Description

The seamless steel gas cylinder which burst is identified as follows, according to information supplied by Mr. A. J. Mallen. Some of the information was obtained from the revised July 25, 1977 test report:

Specification	DOT 3T
Test Date	June 19, 1977
Date of Test Report	July 6, 1977 (Original Date) July 25, 1977 (Revision Date)
Serial Number	9959
Identifying Symbol	U.S. J.B.K.
Minimum Sidewall	0.470 inches
Marked Service Pressure	2725 psi
Heat Code	A29
Type of Steel	Quenched and tempered - ASTM A-372, Class 5, Type E
Water Capacity	600 Gallons
Size	22-inches Diameter, 34-feet Length

A photograph of the eleven pieces of cylinder 9959 laid out on the floor of the Gladstone Laboratories appears in Figure 2a. A diagram of these pieces appears in Figure 2b. The remainder of trailer T-256 after the incident appears in Figure 3. For comparison, an intact tube trailer is shown in Figure 4.

Review of color photographs of the pieces of cylinder 9959 and visual inspection of the pieces laid out as in Figure 2a did not reveal any signs of heating. Evidently, all pieces escaped significant heating from the fire which occurred shortly after the cylinder ruptured.

2. PURPOSE

1) Evaluate the compliance of cylinder 9959 with those requirements of specification DOT 3T which relate to:

- steel chemistry
- tensile properties
- Charpy properties
- wall thickness
- surface hardness of the cylindrical section

2) To identify the cause of the burst of cylinder 9959. As will become evident, this has involved a wide range of investigative activity, including:

- natural gas sampling and analysis
- fractographic and metallographic examination
- electron microprobe analysis
- hardness testing and microhardness testing
- K_{ISCC} testing (a fracture mechanics stress corrosion test)
- stress analysis via fracture mechanics

3. COMPARISON OF TEST RESULTS WITH REQUIREMENTS OF SPECIFICATION DOT 3T

3.1 Chemical Analysis

Chemical analysis was carried out on a specimen cut from piece RR-12. Drillings were obtained from the piece labeled "Chem" in Figure 5. One analysis was handled by the Gladstone Laboratories and another was handled by NBS. In both instances, material was sent to analytical laboratories which rely on NBS Standard Reference Materials for calibration. Results appear in Table I. The scatter between the two sets of chemical composition determinations is not unreasonable for routine chemical analyses of the same material. Also appearing in Table I is a tabulation of the specification requirements. It is clear that these results comply with the chemistry requirements in Section 178.45-5 of Specification DOT 3T. These results are also consistent with results appearing in the independent inspector's report.[2]

The relatively low level of sulfur reflects favorably on the steelmaking process. Low levels of sulfur favor good toughness.

The carbon level suggests strong responsiveness to hardening by quenching and tempering.

Residual elements are cited in Table II. The copper and nickel contents are well within the guidelines suggested in the American Iron and Steel Institute's Steel Products Manual,[6] a widely-recognized specification for the chemistry of steels.

The aluminum level in Table II suggests that deoxidation was accomplished with aluminum. A benefit from deoxidation with aluminum is the formation of fine austenite grains (probably ASTM 7-8) which are

desirable from the standpoint of heat treatment and mechanical properties. The low titanium level suggests that titanium was not used for deoxidation.

The nitrogen and oxygen levels are typical for good steelmaking practice.

Arsenic, antimony, tin and phosphorus are well known for their tendency to promote temper embrittlement.[7] It is thought that interactions occur between these elements and alloying elements in low alloy steels to promote embrittlement of grain boundaries. Only trace concentrations (a few parts per million) are needed. Temper embrittlement of this particular steel specimen from arsenic, antimony and tin is not ascertainable, because the concentrations of these elements fall below the limits of detectability. However, the phosphorous level is close to the range thought to be critical for promoting temper embrittlement in alloy steels containing chromium and manganese.[7] This point is mentioned again in Section 4.3.5.

3.2 Tensile Properties

3.2.1 Test Results

Several tensile specimens were prepared and tested in accord with Section 178.45-13 of Specification DOT 3T. Both longitudinal and transverse specimens were tested. Gage length was two-inches. Nominal width of the gage section was either 0.5 or 1.5-inches. Nominal gage thickness was the full wall thickness. The inside and outside wall surfaces were not machined.

Pieces of the burst cylinder were distorted, as shown in Figure 2. Thus, when necessary, material from which test specimens were machined was flattened at room temperature in a press before machining the tensile

specimens. Cold work introduced during catastrophic failure or flattening would have the tendency to raise the strength of the material. Yield strength is usually more sensitive to cold work than is tensile strength.

Tensile test specimens were taken from two pieces of the burst cylinder -- piece RR-12 and piece RR-10. Piece RR-12 was chosen because it contained one side of the fracture origin. Piece RR-10 was selected because it was remote from the fracture origin. There was no evidence of heating from fire or any other source on these pieces.

Tensile test results appear in Table III. There is a large variation in tensile properties. The range in properties of longitudinal specimens is listed below. Tensile test results from the Battelle reports are also listed.

	Range			
	NBS	Gladstone	Battelle	
Property	Rectangular	Rectangular	Rectangular+	Rounds*
Yield Strength (psi)	114.6 - 138.0	114.0 - 148.0	148.7	105.6 - 143
Tensile Strength (psi)	150.3 - 165.0	136.5 - 170.5	170.5	139.4 - 162
% Elong. in two-inches (t x 1/2)	13.6 - 16.4	13.0 - 17.5	13.0	12.8 - 18
% Elong. in two-inches (t x 1 1/2)	16.0 - 19.8	---	---	---

*Specimens were 0.25-inches diameter by 1-inches long.
+Only one rectangular specimen was tested.

Results from all three laboratories are consistent with one another in that they cover about the same range. The range for these results is broader than is customary in production tensile testing of uniform material, and it is concluded that these results indicate significant material variability in cylinder 9959.

3.2.2 Specification Requirements

In Subparagraph 178.45-15-(a)-(1) of Specification DOT 3T, it is stated that, "The tensile strength may not exceed 155,000 psi." Four of

the nine longitudinal tensile strengths listed in Table III exceed this limit.

Many of the tensile strengths listed in Table III are higher than the tensile strengths cited in the independent inspector's report.[2] The data in the inspector's report are usually obtained from specimens taken from a test ring made from the same heat of steel from which the cylinder is manufactured. The test ring is heat treated along with as many as five cylinders. Properties measured on specimens from the test ring presumably are representative of all cylinders made from the same heat of steel. The observed differences in tensile strength may be accounted for in part by material variability.

In Subparagraph 178.45-15(a)(2) of Specification DOT 3T, it is stated that, "the elongation must be at least 16 percent for a two-inch gage length." This requirement was met for the test specimens in Table III which had a width of 1 1/2 inches. This width is within the range specified for tensile specimens and favors high elongation.

All of the elongations listed in Table III are lower than the elongations cited in the independent inspector's report. As in the case of the tensile strength differences, material variability may account in part for the observed differences in elongation.

For purposes of comparison, two longitudinal tensile test specimens were obtained from another cylinder, 10041, which was also on trailer T-256. The specimens were prepared and tested in accord with Section 178.45-13 of Specification DOT 3T. The cross-section was 1.5-inches x 0.480-inches, and the gage length was two-inches. These specimens were tested along with the specimens which gave the results in rows 3, 4 and 5 of Table III. Results appear below:

Specimen Identification	Yield Strength (psi)	Tensile Strength (psi)	% Elongation in Two Inches
1-1	123,000	143,000	22.6
1-2	122,000	142,000	24.6

It is clear that these results conform with the tensile strength and elongation requirements of Specification DOT 3T.

3.3 Charpy Properties

Full-size Charpy specimens were prepared and tested in accord with Section 178.45-13 of Specification DOT 3T. Test temperature 0 °F. Both longitudinal* and transverse* specimens were tested (There is no specification requirement on transverse Charpy specimens). Specimens were taken from two pieces of the burst cylinder -- piece RR-12 and piece RR-10E. These pieces were selected to provide data from material close to the fracture origin and remote from it. There was no evidence of heating on these pieces. By judiciously selecting reasonable flat pieces, it was not necessary to flatten the material from which test specimens were machined. The effect on the Charpy data of the flattening during the rupture is unknown.

Results appear in Table IV. The data indicate that the material from piece RR-10E is somewhat tougher than the material from piece RR-12. As expected, the transverse specimens show less toughness than the longitudinal specimens. This result arises because the crack in transverse specimens propagates parallel to elongated sulfide inclusions and regions of banding, both of which are zones of low fracture resistance. These features of the microstructure develop parallel to the drawing direction during fabrication of the seamless tube and are not easily eliminated.

---

*Longitudinal Specimen: Axis of specimen parallel to axis of cylinder and crack propagating circumferentially.

Transverse Specimen: Axis of specimen in circumferential direction and crack propagating parallel to axis of cylinder.

Requirements of specification DOT 3T for full size, longitudinal Charpy specimens appear in Table IV. Absorbed energies for the longitudinal Charpy specimens from piece RR-12 do not meet the specification requirements, whereas results on the longitudinal specimens from piece RR-10E do meet the specification requirements.

Energies for longitudinal Charpy specimens from piece RR-12 are lower than energies cited in the independent inspector's report. On the other hand, energies for longitudinal specimens from piece RR-10E are comparable with results in the inspector's report.

These Charpy test results are comparable to results in the Battelle Report.[5]

3.4 Wall Thickness

In the revised test report, July 25, 1977, the minimum wall thickness was cited as 0.470-inches. This is the required minimum wall for marked service pressure of 2725 psi, as determined under Section 178.45-7 of Specification DOT 3T. Wall thickness measurements were made with a hand-held micrometer at various positions along the fracture surface evident in Figure 2a. Typical measurements ranged between 0.458 and 0.472-inches. Slight thinning may occur close to the slant fracture surface due to stretching during ductile fracture. Hence, these measurements may not give an accurate indication of the as-manufactured wall thickness. It is noted that these measurements are generally below the required minimum wall, 0.470-inches.

Wall thickness measurements also show up in Table III, where each first number in the third column represents the full wall thickness. These thicknesses are representative of the as-manufactured thickness, since they are from regions remote from the slant fracture surface. These thicknesses are generally below the required minimum wall, 0.470-inches.

3.5 Surface Hardness of the Cylindrical Section

Surface hardness was measured in accord with Subparagraph 178.45-15 (a)(4) of Specification DOT 3T. Results appear below.

Location	Rockwell C-Scale Hardness Below Decarburized Layer (0.033-inches below surface)
Piece RR-12 (near fracture origin)	34.5
Piece RR-17	33

These results fall below the specification allowable maximum of Rockwell C-36, indicating that this requirement of the specification was met.

4. FRACTURE DESCRIPTION

4.1 Location and Description of Fracture Origin

The cylinder which ruptured was in the top row of a four-wide by three-high array of cylinders on the tube trailer. It was on the outside at the right, as viewed from the rear of the trailer, Figure 6. The serial number stamped in the cylinder is 9959. For convenient reference to positions of cylinders on the tube trailer, the cylinders are numbered 1 through 12, as shown in Figure 6. Thus, the cylinder which ruptured is also designated as cylinder 4.

The fracture origin was located in the sidewall of the cylindrical section. It was first identified by R. McCombs of the Gladstone Laboratories, and subsequently verified by B. W. Christ of the National Bureau of Standards and W. A. Maxey and T. Groeneveld of Battelle. It was about 12.5 feet from the front head, and between the 6 and 7 o'clock positions*, as shown in Figure 6. THe fracture origin was between pieces RR-12 and RR-16.

The edge of piece RR-12 containing the fracture origin appears in Figure 5. It is located along the fracture edge where the words "saw cut" appear upside down. One side of the fracture origin was removed from piece RR-12 by sawing along the "saw cut" line. The other side has been preserved intact on piece RR-16. Care was exercised in the sawing so that coolant from the band saw did not flow over the fracture surface. A heavy deposit of various products coated the entire fracture surface.

---

*12 o'clock is located at the top of the cylinder, when the tube trailer is viewed from the rear.

The fracture origin was a thumbnail-shaped part-through crack about 1.3-inches long and 0.25-inches deep. It reached from the inside wall to the mid-wall position. The long axis of the crack was approximately parallel to the longitudinal axis of the cylinder.

It is possible that the fracture origin was not a single crack, but rather, three cracks that linked up, as suggested in Figure 7. Figure 7a is an overall view of the 17-inch long segment sawed from RR-12. This segment was about 1/2-inch wide at one end and 3/4-inches wide at the other. The outside wall is facing the viewer in Figure 7a. A view directly down on the fracture origin appears in Figure 7b. Figure 7c is an artist's sketch clarifying Figure 7b and showing the position of the fracture origin on the 17-inch long segment. The step in the fracture origin between labels "1" and "2" is suggestive of 2 cracks. Yet a third crack is suggested by the asymmetry of the fracture origin in the region labeled "3".

Tiny shear lips were noted along the edge of the fracture origin which intersected the inside wall. These show up in Figures 8a and 8b. The presence of a shear lip suggests internal crack growth, with the shear lip forming at the time of catastrophic separation. The shear lip is probably in the decarburized layer (see Section 5.3), which was detected along the inside wall of the cylinder.

Other notable features of the fracture origin include: 1) "flat fracture" radially through the wall thickness at the position of the thumbnail-shaped part-through crack, and 2) a transition from flat fracture to full slant fracture within a few inches longitudinally on either side of the fracture origin. Slant fracture indicates ductile separation, whereas flat fracture indicates separation with little or no ductility.

4.2 Fracture Path and its Relationship to the Site Configuration After the Incident

The primary fracture path is marked by the heavy black lines in Figure 2b. Secondary fracture paths are indicated by the dashed lines. They probably developed in response to bending loads on an already-fractured section of the cylinder.

Numerous flat spots were found along the entire fracture surface of cylinder 9959. The flat spots were usually 1-2 inches long. Their presence shows an intermittent transition from ductile (slant) to brittle (flat) fracture and may indicate numerous small brittle zones throughout cylinder 9959. These observations are consistent with a finding in the Battelle report,[5] namely that drop weight tear test data ". . . indicate a variable material with no consistent transition temperature."

A fast-running shear fracture runs at a velocity of about 1000 to 3000 feet per second.[22] Taking the cylinder length as 34 feet and positioning the fracture origin at 12.5 feet from the front, it is estimated that the primary crack running at 1000 feet/second reached the front of the cylinder in about 12.5 milliseconds and the rear in about 21.5 milliseconds.

Heavy flanges threaded onto the outside of the necks at each end of the cylinder to hold it to the trailer bulkhead acted as crack arrestors. When the primary crack reached each head, it followed a circumferential path along internal threads machined in the neck for manifolding and turned back into the cylinder. There was no evidence that the fracture originated at the internal threads in either head.

Near each head, the fracture path followed forging seams which formed from gathered metal that accumulated when the heads were forged, Figure 9a. Such forging seams were found at the heads of other

cylinders on trailers T-256 and T-254, as determined by visual examination through the 3 1/2-inch diameter openings at each head. Some forging seams were metallographically examined in cross sections taken from the front head of cylinder 10041. These seams were about 1/32-inches deep and were partially filled with a black substance which was not identified. A typical as-polished cross-section is shown in Figure 9b. Etched sections showed that the decarburized surface layer (see Section 5.3) followed the contour of the forging seams, verifying that the contour developed during forging and not afterward. There was no evidence that the fracture of cylinder 9959 originated in the forging seams.

Reference to the incident site diagram in Figure 1 shows that the front head was launched frontward across the gravel road in a line almost parallel to the longitudinal axis of the tube trailer as it sat on the gravel pad. The rear head was propelled rearward at an angle to the tube trailer axis. The reaction force from the rear head's launch may have swung about the rear of the tube trailer and helped to tip it on its side. It is probable that the thrust of the decompression wave propelled the front and rear heads. Piece RR-16 flew along a line almost perpendicular to the longitudinal axis of the cylinder and piece RR-12 landed somewhat rearward to the trailer. These observations are consistent with the position of the fracture origin.

Cylinders 1, 2 and 3, Figure 6, were flung from the trailer in the direction of the compressor. The trailer bulkhead is designed with a separate piece at the top to accomodate installation of each cylinder in the top row, Figure 3. Each separate piece is bolted in place. The sidewards and upwards thrusting forces applied to cylinder 3 from the

longitudinal opening flap of cylinder 4 are probably the primary forces which propelled cylinders 1, 2 and 3 to their final positions. There were numerous circumferential scrape marks on the front half of cylinder 3 between the 10 o'clock and 6 o'clock positions. The bolting of the separate pieces in the front bulkhead, Figure 3, was apparently easily overcome by the rupturing forces, allowing the front ends of cylinders 3, 2 and 1 to readily separate and lift from the trailer. A sidewards impact from the opening flap of cylinder 4 along the front half of cylinders 1 and 2 would spin them end for end, and result in their orientations as shown in Figure 1. The positions in which cylinders 1, 2 and 3 landed are consistent with the position of the fracture origin.

It is likely that the impacts from the frontward opening flap of cylinder 4 along cylinder 3 led to the flexing and bending which developed more secondary crack paths at the front than at the rear of cylinder 4.

The line labeled ABC in Figure 2b shows up clearly as a "hit mark" on cylinder 8, Figure 10a. As expected from the relative positions of cylinders on the trailer shown in Figure 6, this marking is in the quadrant from 9 to 12 o'clock. Furthermore, cylinder 8 is bowed significantly in response to the blow represented by the hit mark, Figure 10b. The position of the hit mark and the bowing suggest that cylinder 4 and 8 were in their normal relative positions at the time of the hit and that 8 was bolted firmly in place at the time of the hit. The blow to cylinder 8 flung it beneath trailer T-264, as shown in Figure 1. These observations are consistent with the position of the fracture origin.

4.3 Other Cracks Near the Fracture Origin

4.3.1 Two Types of Cracks

In addition to the fracture origin, some other cracks were detected in piece RR-12. These other cracks were of two distinct types.

Type C - These are subsurface cracks close to the inside wall. The plane of the crack is roughly parallel to the inside wall. The depth below the inside wall varied from from 0.01 to 0.10-inches. Several Type C cracks were found. As explained in Section 4.3.4, Type C cracks result from diffusible hydrogen entering the steel. Often, Type C cracks are referred to as "Blister Cracks".

Type C cracks were detected in transverse and longitudinal sections. They have their long axis in the longitudinal direction.

Type L - The plane of these cracks is roughly perpendicular to the inside wall. The fracture origin was a Type L crack. As explained in Section 4.3.5, Type L cracks probably result from the hoop stress and other service stresses acting on radial components of Type C cracks. The Type C cracks can be thought of as sources of the Type L cracks. Six Type L cracks were found which had intersected the inside surface.

Type L cracks were detected in transverse sections. Their long axis is in the longitudinal direction.

Some of these other cracks were found at NBS in transverse sections of the 17-inch segment containing the fracture origin, Figure 7. Examples of Type C and Type L cracks appear in Figure 11. This photo shows the right hand face of piece TR-1, as indicated in Figure 7c. Four Type L cracks which intersected the inside wall were discovered by workers at the Gladstone Laboratories. Two of these cracks were examined at Battelle and are described in the Battelle Report.[5] One of these cracks was examined at NBS. The results of these examinations are consistent with one another. Each of these three Type L cracks was similar to the fracture origin, which is described in Section 4.5. The fourth crack remained intact at the Gladstone Laboratories. A summary of the cracks found in piece

RR-12 appears in Table V. Visual examination of all the other pieces of cylinder 9959 did not reveal additional cracks intersecting the inside wall.

Visual examination and random metallographic sectioning did not reveal either Type C or Type L cracks in other pieces of cylinder 9959. Nor were such cracks found in the few randomly selected sections of cylinder 10041 which were examined. Nevertheless, there might be other cracks in the remains of cylinder 9959. For the sake of providing a complete picture of the distribution of cracks, it would be informative to search the inside wall of cylinder 9959 for additional cracking using non-destructive inspection techniques. Ultrasonic testing and magnetic particle testing would be appropriate. Searching other cylinders on trailers T-256 and T-254 would also be appropriate.

4.3.2 Etching to Reveal Banding

Etching of transverse sections revealed a feature of the metallurgical structure called banding. The Type C cracks often were detected in white-etching banded regions which were near the inside wall. An example of a Type C crack in a banded region appears in Figure 12. Etching with 2% nital* or nital with an ammonium molybdate additive** revealed the banding. Etching with the additive gave a sharper definition of the microstructural features.

Banding is a well known feature of the metallurgical structure of wrought commercial steels. Banding refers to microzones which have variable chemistry. The origin of banding is chemical segregation

---

*2% nital consists of 2 ml. of nitric acid and 98 ml. of ethyl alcohol.

**Nital with the ammonium molybdate additive is prepared as follows: 100 ml. ethyl alcohol mixed with 2 ml. of the following solution - 15 gm. ammonium molybdate dissolved in 100 ml. water and mixed for four days with 100 ml. nitric acid.

which occurs during solidification of the ingot. Such segregation occurs in the last regions of the ingot to solidify, which are along the centerline and near the top. The segregation is explainable from phase diagram considerations, which show that the last liquid to solidify is enriched in alloying elements.[8] When a tube round* is rolled from an ingot, the enriched regions are stretched out longitudinally along the centerline. Elongated banded regions result. The geometry is as if stacks of tiny, wavey playing cards were embedded in the cylinder wall, with the long axis of the cards parallel to the long axis of the cylinder. Piercing and roll forging the tube round to make the seamless cylinder tends to elongate banded regions longitudinally still more. Because the tube round is pierced along its centerline, the banded regions with the most severe chemical segregation remain close to the inside wall. Banding cannot be eliminated by conventional heat treatments.

Electron microprobe analysis was carried out to characterize the microchemistry of the white-etching microzones. Specimen L in Figure 7c was selected for this examination. The microzone examined appears in Figure 13. Results are listed in Table VI. No carbon segregation was detected. Nor was sulfur segregation found. Phosphorus was the most intensely-segregated element, followed by chromium and molybdenum, and then manganese and silicon. Such microsegregation is probably typical in all the white-etching microzones.

4.3.3 Microhardness in the Banded Regions

Microsegregation can contribute to high hardness through solid solution strengthening, precipitation hardening and resistance to softening during

---

*"Tube round" is steel mill terminology for the semi-finished product resulting from rolling a 15 to 20 ton ingot into starting material for the seamless tube mill. Tube rounds are solid cylinders a few feet long with diameters up to 14-inches.

tempering. A survey of microhardness was carried out in order to determine if the hardness of the white-etching microzones in which the Type C cracks occurred was different from the hardness of the surrounding material. Five transverse sections were examined. They are labeled TR-1, TR-2, TR-3, TR-5, and R in Figure 7c. Results appear in Table VII. The white-etching microzones were significantly harder than the surrounding material, as illustrated in Figure 3. Often, the Knoop microhardness measurements in the white-etching microzones converted to Rockwell-C scale hardnesses of 40 or greater. For comparison, the surrounding material was softer and exhibited equivalent hardnesses on the Rockwell C scale of 35 to 40.

Material from other pieces than the piece in Figure 7 was examined metallographically and tested for microhardness. One transverse section came from the left-hand end of the segment labeled "D" in Figure 5. Three transverse sections came from a ring section cut from within a foot of the front head of cylinder 10041. (See Figure 6) Results from these specimens appear in the last four rows of Table VII. One finding from the metallographic work was that the banded regions in these four specimens did not etch as white as the banded regions in the other specimens. Light-dark etching did occur in these last four specimens, and it provided the contrast which revealed the banding, Figure 14. As shown in Table VII, the Rockwell C-scale equivalent of the Knoop microhardness measurements for these four specimens was around 30 $\pm$ 3. Microhardness was somewhat higher in the light etching bands.

It is not clear why the banded regions in the last four specimens listed in Table VII did not show the sharper white contrast or the higher hardness found in the other specimens. The lower values of microhardness for the last four specimens suggest that the amount of chemical segregation is less.

4.3.4 Explanation of Type C Crack Formation

Hard microzones in banded steel are often susceptible to cracking in the presence of diffusible hydrogen.* A widely-accepted rule of thumb is that susceptibility increases with increasing hardness.[9] Although researchers disagree among themselves about the details of hydrogen-assisted cracking mechanisms, there is general agreement that hydrogen is attracted to preferred sites in steel, e.g., hard microzones, and causes internal cracking, sometimes called "blister cracking." The internal cracking is often attributed to extremely high internal hydrogen gas pressure which develops when diffusible hydrogen atoms, H^o, recombine to form molecular hydrogen, H_2[17]. Thus, a high level of externally-applied stress is not required for such cracking. The key factors for promoting hydrogen-assisted cracking are a susceptible microstructure and a source of diffusible hydrogen.

The natural gas being pumped into cylinder 9959 at the time of rupture contained about 500 ppm by volume of hydrogen sulfide at the inlet to the compressor. (See Section 6.2) It is well known that hydrogen sulfide gas can react with steel at ambient temperatures to produce diffusible hydrogen.[11] A simplified expression for the decomposition reaction is[11]

$$H_2S + Fe \rightarrow FeS_x + 2H^o$$

The presence of liquid water favors this reaction.[11] Iron sulfide produced by this reaction, FeS_x, generally adheres to the steel surface

---

*Diffusible hydrogen means atomic hydrogen, H^o. The hydrogen molecule, H_2, is too large to diffuse appreciable distances in short times in steel. However, the H^o species could saturate a 0.050-inch diameter steel cylinder in about a minute at room temperature. (Ref. 11) Impediments to diffusion could increase the saturation time to about 5 days at room temperature.

as a black substance, such as that appearing in Figure 21. Sulfur signals were obtained via electron microprobe analysis from this region of the fracture origin (See Section 4.5), suggesting that the black substance in Figure 21 is iron sulfide. Hence, the evidence suggests that a source of diffusible hydrogen was was present.

Guidelines issued by the National Association of Corrosion Engineers[13] suggest that 500 ppm hydrogen sulfide in natural gas is more than sufficient to promote sulfide stress cracking in a steel with a Rockwell C-scale hardness of 40. Such gas is termed "sour gas." A conclusion to be drawn from the foregoing information is that the Type C cracks found in hard, white-etching microzones in transverse sections of cylinder 9959 resulted from hydrogen-assisted cracking.

Sulfide inclusions are another preferred site for internal cracking in steels. An example of hydrogen-assisted cracking in a laboratory specimen from cylinder 10041 (see Figure 6) appears in Figure 15. In this case, the specimen was saturated with diffusible hydrogen from an aqueous acidified solution saturated with hydrogen sulfide,[14] which is known as a severely corrosive solution. The low pH of this solution favors the entry of hydrogen. Some cracks in Figure 15 have formed along sulfide inclusions in the absence of an externally-applied stress.

4.3.5 Explanation of Type L Crack Formation

It is likely that the Type L cracks developed as a result of the hoop stress and other service stresses acting on radial jogs in the Type C cracks. An example of an incipient Type L crack forming as suggested appears in Figure 16. This mechanism of formation is consistent with the observations that the Type L cracks often intersect Type C cracks. For example, as shown

in Section 4.5, the fracture origin (which is a Type L crack), has intersected a Type C crack, Figure 22a. In the Battelle study,[5] a Type C crack was found at about the mid-point of a Type L crack, as shown in their Figure 15.

An interesting aspect of the growth of Type C cracks is shown in Figure 12b. The crack tip is shown at a magnification of 800X. The crack path is intergranular. It may be that the prior austenite grain boundaries have undergone temper embrittlement and that hydrogen-assisted intergranular crack growth is thereby aided.[7] In any case, the jog formed in the Type C crack can be acted on by the hoop stress and other service stresses, and thereby serve as a starter for a Type L crack.

The presence of diffusible hydrogen could easily assist the growth of Type L cracks when they form as subsurface cracks. Once a Type L crack penetrates the inside wall, any harmful chemical species in the cylinder could assist in promoting further growth. Hence, the Type L cracks may have grown via two distinctly different processes:

1) Hydrogen-assisted crack growth while subsurface.
2) More general stress corrosion by any harmful chemical species, once the inside wall is penetrated.

The Type L cracks examined in this study are not tight. The crack openings are rather wide, typically 0.0004 to 0.004-inches. An extremely wide Type L crack appears in Figure 11. It is possible that the Type L cracks were tighter in the intact cylinder and that these cracks widened during the catastrophic rupture.

4.3.6 Summary of Cracking in Cylinder 9959

Reference to Figure 7 and Table V shows that the cracking detected in piece RR-12 was localized to the vicinity of the fracture origin.

Furthermore, cracking was not detected in other pieces of cylinder 9959. The general impression from metallographic examination and microhardness testing is that regions of piece 12 of cylinder 9959 exhibit exceptionally high hardness and microchemical segregation. Such regions occasionally occur during steelmaking and fabrication. They originate from chemical segregation which occurs during the solidification of the ingot. (See Section 4.3.2).

In the case of a cylinder containing a harmful chemical species, there may be direct contact between the chemical species and banded regions which are highly susceptible to environmentally-assisted cracking. In the case of cylinder 9959, the diffusion path between the harmful chemical species (diffusible hydrogen, H^{O}, from the decomposition of hydrogen sulfide) and the highly susceptible microstructures (hard, white-etching microzones beneath the inside wall) was about 0.01 to 0.1-inches.

4.4 Examination of Inside Wall

4.4.1 Surface Topography

Adhering soil and other products coated the inside wall of the pieces of cylinder 9959. To the eye, these inside surfaces appeared brown and rusty. Some regions of the inside wall were cleaned by workers at the Gladstone Laboratory with a soft bristle brush to facilitate visual examination. Further cleaning was done on pieces examined at the Bureau of Standards. Ultrasonic cleaning in petroleum ether, and solution cleaning with ammonium citrate* or buffered hydrochloric acid** solutions were the

---

*Ammonium citrate cleaning solution: This is a saturated aqueous solution of ammonium citrate.

**Buffered hydrochloric acid solution: 3 ml HCl, 4 ml 2-butyne-1, 4 dial, 50 ml deionized H_2O. This cleaning solution tends to minimize the solution of substrate metal.

methods used to prepare surfaces for microscope examination. Not all inside wall surfaces of the pieces from cylinder 9959 were cleaned. The focus for cleaning was on piece RR-12. Specific mention is made in the text when the surface under discussion was solution cleaned. Otherwise, the surface was examined after bristle brushing.

Many transverse sections were taken near the fracture origin (see Figure 7c) to examine the integrity of the inside wall and the surface pofile of the inside wall. Generally, the surface profile was rough and uneven. Sometimes such roughness is due to surface laps. Occasionally, surface laps form along the inside wall during manufacture. These laps result when oxide scale is pressed into the wall during hot forming. An example of a surface lap appears in Figure 17. It was found at NBS during examination of a transverse section from cylinder 10041. No surface laps were detected in the NBS study of cylinder 9959. However, one was found at Battelle Memorial Institute during examination of a specimen from piece RR-12. There was no indication that surface laps caused the fracture.

An unexplained pattern of sets of parallel circumferential lines was embossed on the inside wall of piece RR-12. These lines were also seen on other pieces and in other cylinders on Trailers 256 and 254. About 7-8 lines were in each set. In Figure 18a, one set runs through the upside-down "R's." The systematic nature of these lines suggests they are related to the manufacturing process. There was no evidence that the fracture was due to these lines.

Generally, the surface of piece RR-12 was uneven, pitted and pockmarked, as shown in Figure 18. The region of piece RR-16 near the fracture origin

was similar. The inside wall of other pieces from cylinder 9959 were not as uneven and pockmarked. The inside wall of a ring taken from near the front end of cylinder 10041 was smooth in comparison to that of RR-12. The general impression from comparison between the inside walls of RR-12 and RR-16, and other pieces, was that the topography of much of pieces RR-12 and RR-16 near the fracture origin was a shade rougher and more marked up by grinding scratches.

It may be more than coincidence that the fracture origin was in the vicinity of this rough surface. For example, the surface depressions could have acted as "potholes" and held liquid water.* There was a strong possibility that liquid water was present, as noted in Section 6.3. In Section 4.3, it was mentioned that liquid water facilitates the decomposition of hydrogen sulfide to form diffusible hydrogen.

Some of the uneven surface topography of piece RR-12 appeared to be grinding scratches. One example is above the marking "PT" in Figure 18a. Normal manufacturing practice involves reaching inside the 3 1/2-inch hole in the cylinder head with a long-handled pneumatic grinder to remove surface discontinuities detected during ultrasonic testing of the finished cylinder. This grinding is intended to remove stress concentrations and notch effects.**

---

*As noted in Section 4.1, the fracture origin was located between the 6 and 7 o'clock positions, as shown in Figure 6. The cylinder is fixed to the trailer, so the fracture origin location was at the bottom where liquid water could accumulate.

**"Notch effects" is terminology used in mechanical metallurgy to describe the tendency of stress concentrations near sharp corners to promote brittle fracture. Ferrous materials are often evaluated for their "notch sensitivity" via the Charpy test.

Microscope examination of regions on the inside surface of piece RR-12 revealed two more interesting features of topography, 1) craters at low magnifications, and 2) an uneven appearance at high magnifications. Observations are shown in Figures 19 and 20.

The region shown in Figure 19 at a magnification of 24 times is the inside wall of specimen TR-1 (see Figure 7c for location) after ultrasonic cleaning and cleaning with ammonium citrate. The valleys running from top left to lower right are grinding scratches. The hemispherical craters probably formed from a shot peening procedure used in manufacture to remove oxide scale from the inside wall.

Figure 20 shows the general uneven appearance of some regions of the inside wall of specimen TR-5 (see Figure 7c for location) after solution cleaning. A strip of remaining corrosion product runs from top left to lower right in Figure 20. Hemispherical craters like those in Figure 18 are also evident in Figure 20a. Figure 20b shows a close-up of one of the uneven regions. Cross-sections through some of these regions revealed that the penetration was limited to less than 1/32-inches. In general, the uneven regions are suggestive of chemical reactions occurring at the inside wall. The Type C cracking discussed in Section 4.3 of this report suggests that one of the chemical reactants might be hydrogen sulfide.

4.4.2 Evidence of Sulfur

Evidence of sulfur-bearing chemical species on the inside wall of cylinder 9959 was found by four independent methods. The sulfur-bearing species probably resulted from the decomposition of hydrogen-sulfide, as discussed in Section 4.3.4. Detection methods included: 1) sulfur printing, 2) sodium azide testing, 3) electron microprobe analysis, and 4) x-ray diffractometry.

Workers at Gladstone Laboratories used the sulfur printing method, which is often used to detect sulfide inclusion distributions in steel ingots. They reported to NBS that a survey of pieces from one end of cylinder 9959 to the other via the sulfur printing technique resulted in strong indications of sulfur. The surfaces examined were on pieces RR-9 (front head), RR-12 (about 12 feet from front head), and RR-10 (rear head). A sulfur print made on the front head of cylinder 10041 also gave strong sulfur indications. The surfaces were cleaned by bristle brushing, and also by rubbing with 180 grit abrasive paper and wiping with a solvent. It was reported that in general, the abraded surfaces gave more intense sulfur prints than the bristle-brushed surfaces.

Sodium azide testing is a chemical solution method used for quick determinations of the presence of sulfur. The region to be examined is exposed to a solution to promote dissolving and the scent of hydrogen sulfide is taken as an indication that sulfur is present. Workers at Battelle Memorial Institute used this method on a section of piece RR-12. They concluded that sulfur was present.[5]

Electron microprobe analysis was carried out at the National Bureau of Standards to search for sulfur-containing compounds. In this method, characteristic x-ray signals from atoms excited by x-ray bombardment serve to identify the chemical species. Caution must be used in this procedure to sort out ambiguities from x-ray lines at nearly-identical energies which come from different kinds of atoms. For example, sulfur, molybdenum and lead have nearly the same emission energies, as indicated in the tabulation below:

Element	Characteristic X-ray	Emission Energy in KeV
Sulfur	K_{α}^{1}	2.308
	K_{α}^{2}	2.306
	K_{β}^{1}	2.464
Molybdenum	L_{α}^{1}	2.293
	L_{β}^{1}	2.395
	L_{β}^{2}	2.518
Lead	M_{α}^{1}	2.346
	M_{β}^{2}	2.443

Suitable analysis procedures coupled with the use of high-resolution spectrometers can overcome ambiguities in the analysis of electron microprobe data.

Electron microprobe analysis was carried out on the inside wall of two specimens from piece RR-12. A transverse section of piece RR-8 (see Figure 7c) was examined. This specimen was placed in a metallographic mount, after inside wall surface cleaning involving light bristle brushing and ultrasonic cleaning in petroleum ether. Four linear scans were made along paths starting in the steel, progressing through the surface product and ending in the mounting material. In the metal, the sulfur signal was insignificant. Strong signals from sulfur were detected as the beam entered the surface layer for all four scans. Potassium, silicon, and aluminum signals were also detected at the location of the surface product. Presumably, these signals were from adhering soil.

The other specimen examined in the electron microprobe for sulfur-bearing species on the inside wall was the piece containing the fracture

origin. (See Figure 7c). A region of the inside wall was examined in nine places. Bristle brushing was the only surface clean-up technique used initially. The predominant signals detected were from iron and silicon, with low intensity signals from sulfur, chromium, manganese, aluminum, potassium and calcium. After cleaning the surface via replica stripping, the signal intensity was variable. Strong sulfur, iron, silicon, chromium, aluminum, potassium and calcium signals were detected in some places, but not in all locations sampled. These results suggest that some soil remained on the inside wall after the replica stripping. They also suggest that the sulfur distribution was non-uniform.

It was thought that some of the sulfur signals may have come from fertilizers in the soil. To examine this possibility, a light scratch was made in a corner of the specimen with a jewelers screwdriver. The scratch removed surface product and revealed bare metal. The intensity of the sulfur line from the scratch increased substantially. This result suggested the presence of a heavy, adherent layer of sulfur-bearing chemical secies along the inside wall near the fracture. This result is consistent with results from sulfur prints of abraded surfaces obtained by workers at Gladstone Laboratories.

X-ray diffractometry was used to search for sulfur bearing species on the piece containing the fracture origin (see Figure 7c). Chromium radiation was used with a pyrolytic graphite monochromator. Initially, the surface was cleaned via bristle brushing and ultrasonic cleaning. Patterns from alpha quartz and the gamma-Fe_2O_3 were detected. After vigorous cleaning the inside wall in the ultrasonic cleaner, the alpha quartz pattern disappeared but the gamma Fe_2O_3 pattern remained. In addition, indications of metal sulfide patterns showed up.

The alpha quartz pattern was probably from adherent soil particles. These x-ray results indicate that soil particles obscured the pattern from metal sulfides which were adhering to the inside wall along with gamma-Fe_2O_3.

4.5 Examination of Fracture Origin

A description of the as-received fracture origin was presented in Section 4.1. Views of the fracture origin appeared in Figure 7. As noted in Section 4.1, the half of the fracture origin on piece RR-12 was examined. The other half remained on piece RR-16.

The fracture origin was examined using the techniques of optical microscopy, scanning electron microscopy and electron microprobe analysis. A view of the as-received fracture surface viewed from the inside wall appears in Figure 8a. The fracture surface was heavily coated with soil and other products. Initially, the fracture surface was cleaned by stripping cellulose acetate replicas. The surface in Figure 21 developed after stripping away 3 replicas. Further clean up efforts with replica stripping were abandoned because the process was slow and tedious. The fracture surface was then cleaned using a buffered HCl solution.* A portion of the cleaned fracture surface containing the step appears in Figure 22a. Occasional regions with surface product remained, but in general, the fracture surface exhibited a dull metallic luster at this stage. Some interesting details were revealed.

The dark horizontal line in Figure 22a is a Type C crack. It is marked in the figure. This Type C crack occurs at the same depth below the inside wall as the Type C cracks discussed in Section 4.3, i.e., between

---

*See Footnote on p. 27 for composition.

about 0.01 and 0.10-inches. Finding a Type C crack at the fracture origin is consistent with the interpretation of Type C and Type L cracks in Section 4.3. To the left of the Type C crack at 0.026-inches below the surface in Figure 22a is a saucer-like depression (evident in stereographic views) which may be the site where a Type L crack developed from this Type C crack.

The possibility of the fracture origin being three independent Type L cracks which linked up was discussed in Section 4.3. The step between regions 1 and 2 of the fracture origin (see Figure 7c) may represent the link-up of two Type L cracks which emerged from radial jogs located at two different circumferential positions on two different Type C cracks. Region 3 may differ from region 2 on the fracture origin because each Type L crack represented by these regions originated at a different Type C crack.

The thumbnail-shaped fracture origin is macroscopically flat. Typical surface topography in this region is shown in Figure 22. The topography might be likened to numerous plateaus and valleys. Figure 22b at a magnification of 250 times is a closeup view of the same structure.

Beyond the thumbnail region --- longitudinally and radially towards the outside wall --- was a very different surface structure. Here the surface was quite rough on a macroscopic scale. It exhibited a texture with directionality in the longitudinal direction. Tiny shear lips were evident along the outside wall. Presumably, this region beyond the thumbnail region represents the remaining ligament which failed in a short time, e.g., milliseconds to seconds, due to tensile overload.

The fine details of surface structure in Figure 22 are probably not representative of what the fracture surface was like when the fracture

origin formed. It is likely that corrosion during the lifetime of this fracture surface obscured most of the origin surface topography. The buffered cleaning solution used to remove adherent surface product may also have contributed slightly to the loss of original topography, and also to a slight exaggeration of the opening of the Type C cracks. These slight modifications have no effect on the major observations or conclusions.

Electron microprobe analysis was carried out in three locations on the fracture surface after the surface was cleaned by stripping 3 replicas. These locations are labeled A, B and C in Figure 21. Strong sulfur signals were emitted from each region. The emission of sulfur signals from the fracture surface suggest that the fracture origin penetrated the inside wall over at least part of its length for some period of its lifetime.

After making the examinations of the as-received fracture origin as described above, a transverse section through the fracture origin was prepared. The objective was to look for hard, white-etching microzones and Type C cracks such as those appearing in Figures 11, 15 and 16. The cut was made as shown in Figure 7c. The piece containing the step was examined on its transverse face via optical microscopy at six successively-deeper levels as the face was ground away.

Hard, white-etching microzones were found at all six levels. Three Type C cracks were found. An example showing two within 0.6-inches of the fracture origin appears in Figure 23a. These type C cracks are within the banded region close to the inside wall.

Figure 23b is a close-up of the region containing the Knoop hardness indentations which appear at the upper right in Figure 23a. The white-etching

microzones are evident in Figure 23b. The hardness at each indentation is listed below.

MICROHARDNESS AT KNOOP INDENTATIONS
APPEARING IN FIGURES 23a AND 23b

Location	Knoop	Rockwell C-scale Equivalent
G-in white microzone	452	44
B-in white microzone	439	43
I-in white microzone	430	42.5
E	424	42
C	418	41
A	394	39
F	392	39
D	383	38
H	378	38
0.3 inches below inside wall	373	37

These results indicate that the region of the fracture origin had a banded microstructure near the inside wall which was highly susceptible to Type C cracking as discussed in Section 4.3.

5. MATERIAL DESCRIPTION

5.1 Grade of Steel and Heat Treatment

The chemistry of the steel used under Specification DOT 3T is listed in Table I. This chemistry corresponds to grades known as ASTM-A372, Class 5, Type E and AISI 4145. This low alloy steel is a high strength pressure vessel steel which is usually used in the quenched and tempered condition.

The heat treatment for 3T cylinders is described in Specification DOT 3T. In Subparagraph 178.45-8(a)(1), it is noted that the steel temperature on quenching must never exceed 1750°F and in Subparagraph 178.45-8(a)(2), it is noted that after quenching each cylinder must be reheated to a temperature not less than 1050°F.

All 3T cylinders are heat treated after the heads are forged. Normal practice involves heating as many as five cylinders simultaneously in a car-bottom furnace. The ends of the cylinders are plugged during heat treatment. Temperature is monitored at about five positions in the cylinder array during austenitizing and also during tempering. Cylinders are quenched in a turbulent oil bath one at a time. Transfer time from furnace to quench bath is about one-minute. Tempering involves heating as many as five cylinders simultaneously in a car-bottom furnace, followed by air cooling. During heat treatment, cylinders are supported at several positions along their length to minimize shape distortion.

A "test ring" is heat treated with each batch of cylinders, in accord with Specification DOT 3T. A test ring may be 18-inches long and is the full diameter and wall thickness of the cylinders. Its ends are

sealed. Specimens are taken from the ring for tensile testing and Charpy testing. Each test ring represents a different heat of steel from the current stream of 3T cylinder production.

5.2 Microstructure from Heat Treatment

The microstructure which results from quenching and tempering a low alloy steel is usually tempered martensite or tempered bainite. Martensite forms throughout thin sections and as an exterior "skin" on thick sections. Tempered bainite forms beneath the skin.

A typical example of the microstructure found in cylinder 9959 appears in Figure 24. This fine scale, acicular structure shown at a magnification of 1000X is tempered bainite. Similar microstructures were found in all the microscope specimens from cylinder 9959 and cylinder 10041.

5.3 Other Features of Microstructure-Decarburization and Banding

Two other features of the microstructure showed up in transverse sections --- decarburization and banding. These features appear in Figure 25.

The two specimens shown were cut from opposite ends of the segment in Figure 7c. The inside wall of each specimen is towards the middle. An appreciable decarburized layer exists in each piece along the inside wall and the outside wall. Estimated depths are tabulated below and compared with similar observations from the study at Battelle Memorial Institute.

Depth of Decarburized Layer in Specimens From Cylinder 9959

Study	Specimen	Inside Wall	Outside Wall
NBS	L	0.027 inches	0.027 inches
NBS	R	0.020	0.013
Battelle	RR126A	0.026	0.033
Battelle	RR12GC	0.026	0.017

The depths of the decarburized layers exhibit a little variability, but are comparable in the specimens examined. Moreover, these depths are typical for hot worked steel which has been quenched and tempered. The decarburized layer represents a surface region which has lost carbon via diffusion of carbon to the surface and chemical reaction with air or a furnace atmosphere. Decarburization occurs at elevated temperatures.

The microstructure of the decarburized layer is not bainite, but ferrite. Ferrite is extremely ductile. The tiny shear lips along the inside wall in Figure 8 are probably in the ferrite layer.

The banding evident in Figure 25 is more pronounced in specimen R than in specimen L. Banding is evidenced by the vertical streakiness in specimen R. The banding is more intense near the inside wall. These two specimens came from about the same longitudinal line along the edge of piece RR-12. The variation in banding shown by these two specimens which were about 17-inches apart is typical. Banding was discussed in Section 4.3.2.

5.4 K_{ISCC} Characterization

5.4.1 Background

"K_{ISCC}" is notation used in the field of fracture mechanics. This is a field of stress analysis which quantitatively evaluates the influence of cracks on the stress which a structure can safely support. The development of this field during the last thirty years resulted from the widespread recognition that most engineering structures may contain cracks which could lead to failure at average applied stresses well

below the yield stress. The utility of fracture mechanics lies in its potential to predict critical crack sizes in terms of applied stress and resistance to crack propagation. A structure which cracks below the critical size would remain intact, whereas a structure with larger cracks would fail.

Fracture mechanics measures the ability of a material to resist crack propagation in terms of "fracture toughness," signified by "K_{Ic}" for plane strain conditions, and "K_c" for plane stress, and with units of Ksi - $\sqrt{\text{inches}}$. Typical values of fracture toughness for steels may range between 50 and 400 Ksi - $\sqrt{\text{inches}}$. Typical aluminum alloys may exhibit fracture toughnesses in the range, 20 to 100 Ksi - $\sqrt{\text{inches}}$. Fracture toughness can be measured on precracked test specimens in an ordinary tensile testing machine. ASTM Standard Method E 399 - 72[15a] describes plane strain fracture toughness testing of metallic materials.

The concept of "K_{ISCC}" is like that of "K_{IC}" and "K_c". The difference is that "K_{ISCC}" relates to crack growth under stress corrosion conditions. K_{ISCC} is the threshold stress-intensity factor for stress-corrosion cracking under plane strain conditions. Low values of K_{ISCC} signify high susceptibility to stress corrosion cracking. Often, in K_{ISCC} testing, it is not clear if plane strain conditions prevail. In such cases, the K-value is called an "apparent K_{ISCC}."

K_{ISCC} for a given material is less than K_{IC} for that material. For example, in the case of a well-known bridge steel,[15b] K_{IC} was about 50 ksi$\sqrt{\text{in.}}$, whereas K_{ISCC} was about 15 ksi$\sqrt{\text{in.}}$ Another feature of K_{ISSC} is that it decreases with increasing yield strength. To illustrate this point, some data obtained in a laboratory study of AISI 4340 steel are listed below.[16] The variation in yield strength resulted from different heat treatments.

Yield Strength (ksi)	K_{ISCC}(ksi - $\sqrt{in.}$)
130	111
180	26
220	10.5

5.4.2 K_{ISCC} Measurements in the Laboratory

An experiment was carried out to estimate K_{ISCC} for the type of steel used under Specification DOT 3T for tube trailer cylinders. Test specimens were obtained from a ring section cut from cylinder 10041 near the front head. This steel has yield and tensile strengths of 122.5 and 142.5 Ksi, respectively.

A wedge-loaded double cantilever beam test specimen was used, Fig. 26. Specimen thickness was 0.375-inches, which fulfills the requirement in ASTM E399-75[15a] for a valid plane strain test for stress intensities up to 50 ksi$\sqrt{in.}$ The specimens were cut from the ring section such that the long axis of the specimen was parallel to the longitudinal axis of the cylinder. The axis of the crack was perpendicular to the wall thickness, so that the crack grew longitudinally. This orientation was selected to approximate the growth of the type L cracks discussed in Section 4.3.

Each specimen was wedge loaded to a predetermined stress intensity, and immersed in an aqueous acidified solution (0.5 wt. pct. acetic acid in distilled water) saturated with hydrogen sulfide.[14] The idea behind this type of testing is that the crack will grow until the stress intensity falls to the threshold level, i.e., K_{ISCC}. After five days, the specimen was removed and examined for crack growth. When crack growth was detected, a value of K_{ISCC} was estimated. These results may overestimate K_{ISCC}, i.e.,

the true value of K_{ISCC} might have been lower if the specimen had been re-immersed and the crack had been given further opportunity to grow. For these initial estimates of K_{ISSC}, however, it was felt unnnecessary to re-immerse the specimens.

Test results appear in Table VIII. K_{ISCC} for this steel appears to be about 40 ksi - $\sqrt{in.}$ The most valid estimate of K_{ISCC} was from specimen number 5, which was coated with wax to inhibit crack growth into the arms. The determinations from specimens 2 and 6 seem reliable despite the arm cracking which occurred. Clearly, the 35 ksi - $\sqrt{in.}$ applied to specimens 1 and 3 was below the threshold stress intensity. In a given batch of test specimens, it sometimes happens that crack initiation does not occur where it would be expected. This seems to be the case for specimen 4.

The utility of this estimate of K_{ISCC} is that it facilitates an evaluation of hydrogen-assisted crack growth in cylinder 9959. The critical crack size can be roughly estimated from the following equation for flat plate,[9]

$$K^2 = \frac{1.2\,\sigma^2 a}{\phi^2 - 0.212(\frac{\sigma}{\sigma y})^2} \qquad (1)$$

where

K = critical stress intensity

σ = applied stress

a - crack depth

ϕ = crack geometry factor (ϕ^2 varies from 1 for a long, shallow crack to 2.45 for a semicircular crack)

σ_y = yield strength

For a long, shallow type L crack and applied stress at the crack tip equal to the yield stress, a_{cr} is estimated to be 0.07-inches. For a semicircular type L crack and applied stress equal to the yield stress at the crack tip, a_{cr} is estimated to be 0.165-inches. A critical crack size of 0.07-inches or less would be consistent with the size of the radial jogs on type C cracks which are described in Section 4.3 as probably giving rise to the type L cracks.

It is felt that these estimates of a_{cr} approximate roughly the limits on critical crack size. The approximation is rough due to simulating the real case with assumptions, such as assuming a surface crack rather than an embedded crack, and estimating K_{ISCC} from a piece of cylinder 10041 rather than from piece RR-12 of cylinder 9959. The higher yield strength of piece 12, 137.5 ksi vs 122.5 ksi for the piece from cylinder 10041, suggests that a somewhat lower K_{ISCC} would be measured for piece RR-12. This in turn suggests a somewhat smaller critical crack size for piece RR-12.

6. GAS ANALYSIS

6.1 Objective of Gas Analysis

The evidence suggesting that cylinder 9959 ruptured due to environmentally-assisted cracking made it desirable to obtain an analysis of the natural gas being pumped into the tube trailer at the time of rupture. Gas samples were being taken at the time of rupture,[17] and gas analysis had been carried out earlier in the life of the two natural gas wells. However, these analyses were for the heat content of the gas and did not focus on potentially harmful chemical species which might be present at the parts per million level. Consequently, gas samples were taken and analyzed at the request of OHMR-DOT as part of this investigation. The focus was on hydrogen sulfide and moisture concentration in the parts per million range.

6.2 Hydrogen Sulfide Analysis

Samples were taken at the two natural gas wells and at the inlet to the compressor, which was about two miles from the wells. The date was May 9, 1978. The sample containers were aluminum alloy compressed gas cylinders especially designed for sample taking. Less than 24 hours elapsed between the time the gas samples were obtained and the completion of the analysis for hydrogen sulfide. The analysis was carried out in a laboratory where such analyses are done routinely.[18]

Results appear in Table IX. These results indicate that a substantial amount of hydrogen sulfide was present in the natural gas --- enough to classify it as a "sour gas" and cause concern about hydrogen-assisted cracking (also called sulfide stress cracking) of steel. For example,

guidelines issued by the National Association of Corrosion Engineers[13] suggest that 400 parts per million hydrogen sulfide in gas at 2000 psi is sufficient to cause "sulfide stress cracking" in steel of hardness greater than Rockwell C-22. Hardness enters this guideline because of the well established rule of thumb that susceptibility of a steel to cracking increases with increasing hardness.[9]

Another guideline to compare with the amounts of hydrogen sulfide in Table IX is found in the code of Federal Regulations, Title 49, Subparagraph 192.475-(c). This subparagraph of the Federal Gas Pipeline Safety Standard deals with the acceptable gas composition for "pipe-type or bottle-type holders." The upper limit is set at 0.1 grains of hydrogen sulfide per 100 standard cubic feet of natural gas. This converts to about 1.5 parts per million by volume of hydrogen sulfide in pure methane, which is well below the values appearing in Table IX. Thus, comparison with this guideline indicates that the levels of hydrogen sulfide listed in Table IX exceed significantly that allowed for gas pipeline hardware.

The Bureau of Mines Circular 8749, "Analysis of Natural Gases, 1976," was reviewed for possible background information about the hydrogen sulfide content of natural gas at the wellhead.[19] However, this document did not report hydrogen sulfide with sufficient accuracy to be helpful.

Table IX shows that there was a reduction of hydrogen sulfide content between the wells and the compressor. This reduction probably represents reaction of hydrogen sulfide with the gathering lines. There is no reason to believe there would be any significant change in the hydrogen sulfide concentration as it passed through the compressor and into the cylinders.

The gas wells were essentially inactive between November, 1977 and May 9, 1978. It is not known what effect this would have on the hydrogen sulfide concentration. It is possible that dry hydrogen sulfide also reacted with the steel of cylinder 9959 to cause environmentally-assisted cracking. That such cracking can occur has been reported.[20] However, environmentally-assisted cracking by hydrogen sulfide is usually favored by the presence of liquid water.

It is informative to review results of an earlier analysis for hydrogen sulfide. This analysis was done at the request of OHMR-DOT as part of this investigation. Some gas samples were obtained in stainless steel compressed gas containers on March 7, 1978. Analysis was carried out on March 30, 1978 in the same laboratory reporting the results appearing in Table IX.[18] Results of this earlier analysis appear below.

Location	Hydrogen Sulfide Concentration (ppm by volume)
Gas Well-Renfro #1	No H_2S Detected
Gas Well-Renfro #3	315 $\pm$ 25

It is believed that the long time between sample taking and analysis allowed reaction involving hydrogen sulfide, other components of the natural gas and the container itself. The result was a substantial reduction in the hydrogen sulfide concentration. Such absorption of hydrogen sulfide during gas sampling is recognized in U.S. Bureau of Mines Circular 8749.[19]

6.3 Moisture Analysis

The moisture content of the natural gas was 800 ppm, as shown in Table IX.[18] This converts to about 40 pounds of moisture per million cubic feet of natural gas. The saturation concentration for moisture

in natural gas at 72°F and various pressures is tabulated below, as calculated from Reference 21.

Saturation Concentration for Moisture in Natural Gas at 72°F

Pressure(psi)	Concentration (Pounds per Million Cu. Ft.)
400	54.1
2000	17.1
2200	16.3
2500	15.3
2600	15.0

Comparison with data in the table indicates that the moisture content of the gas, 40 pounds per million cubic feet, exceeds the saturation concentration at shipping pressure. In a cylinder holding 16,000 cubic feet of natural gas, about 0.4 pounds of water would precipitate. This result suggests that liquid water was present in cylinder 9959 at the time of rupture. As noted in Section 4.3.4, the presence of liquid water favors the decomposition of hydrogen sulfide, which results in diffusible hydrogen.

As noted in Section 1.1, the pressure in the gas gathering lines was about 400 psi. At this pressure, the moisture in the gas would exist as vapor.

6.4 Other Chemical Species

Other components of the May 9th set of gas samples were analyzed.[18] Results appear in Table X. These results are presented only for the sake of completeness. There is no reason to believe these components of the gas were related to the environmentally-assisted cracking of cylinder 9959.

Carbon dioxide in conjunction with moisture and carbon monoxide is known to promote stress corrosion in compressed gas containers.[22,23] Carbon

dioxide was determined to be 0.01 mole percent at each gas well and at the input to the compressor.[17] It would be helpful to know the carbon monoxide content of the gas, since the possibility exists that crack growth via the CO_2-CO-H_2O mechanism might have occurred when subsurface cracks penetrated the inside wall. It is believed that in the absence of carbon monoxide, the proposed mechanism cannot operate.[22,23]

7. HARDNESS SURVEY

During the course of this investigation, it was convenient to make hardness measurements on numerous specimens from along cylinder 9959 and from other cylinders as well. The objective in making these measurements was to obtain an overview of hardness variations throughout cylinder 9959 and to estimate the variability of hardness among cylinders. These measurements also provide a basis for estimating the susceptibility of the steel to environmentally assisted cracking. A widely-accepted rule of thumb is that susceptibility increases with increasing hardness.[9]

Hardness measurements were made on transverse sections. Rockwell C-scale measurements were made on unmounted specimens with parallel faces. Some measurements were made on the milled shoulders of tensile specimens. Measurements were made carefully to avoid edge effects. Occasionally, a hardness measurement was made on a specimen in a metallographic mount to obtain an approximate value of hardness. Results are reported in standard ASTM notation, e.g., "HRC 22."

There is no requirement in Specification DOT 3T for hardness on transverse faces. Hence, it is not appropriate to compare the hardness measurements reported herein with any part of it.

Results of the hardness survey appear in Table XI. These results were obtained at the National Bureau of Standards and also at the Gladstone Laboratories. These results indicate a variable hardness in piece RR-12. The range is from HRC 31.6 to HRC 39. These results suggest that the hardness of piece RR-12 which contained the fracture origin is somewhat greater than the hardness of pieces RR-10 and RR-17A.

Comparison of all the results on cylinder 9959 with results from the two other cylinders listed in Table XI indicates that cylinder 9959 is somewhat harder than the other two cylinders. It is expected from the comparison of tensile data obtained on cylinders 9959 and 10041 cited in Section 3.2 that cylinder 9959 would be harder.

Following the rule of thumb that susceptibility to environmentally-assisted cracking increases with increasing hardness, cylinder 9959 would be expected to be the most susceptible of the three cylinders listed in Table XI.

Results in Table XI suggested making a further comparison between hardnesses measured on the three cylinders. Hardnesses were measured on the cylindrical surface, as shown in Table XII. These results also indicate that cylinder 9959 is somewhat harder than the other two cylinders. These results show further that meaningful hardness results can only be obtained by grinding away a substantial layer from the outside surface to get below the decarburized layer. Some measurements of the depth of the decarburized layer appear in Section 5.3.

8. STRESS ANALYSIS VIA FRACTURE MECHANICS

8.1 Review of the Fracture Origin

The fracture origin was described in Sections 4.1 and 4.5. It was thumbnail shaped and was about 1.3-inches long and 0.25-inches deep. It may have formed via the link-up of 3 closely-spaced cracks. A notable feature of the fracture origin is that it was macroscopically flat, Figure 23a. Yet, on a microscale, it consisted of plateaus and valleys, Figure 22b. Macroscopically, the fracture origin looked like a brittle fracture. Microscopically, the fracture origin appeared somewhat ductile.

Two analyses have been carried out using fracture mechanics analysis methods to estimate the critical crack size which would result in catastrophic rupture. The analysis in Section 8.2 is for brittle fracture of a structural material with a surface flaw. The analysis in Section 8.3 is for ductile fracture of a cylinder with a through-wall flaw.

8.2 Tiffany and Masters Equation

Tiffany and Masters[24] published a method of fracture mechanics analysis for brittle fracture of structural materials with surface flaws. Their equation is

$$\left(\frac{a}{Q}\right)_{\text{critical}} = \frac{1}{1.21}\left(\frac{K_{IC}}{\sigma}\right)^2 \qquad (2)$$

where

a = crack depth

Q = crack shape parameter

K_{IC} = plane strain fracture toughness

σ = applied stress

K_{IC} for the grade of steel used in 3T cylinders has been estimated in laboratory tests as follows:[25]

Heat Treatment	K_{IC}
Quench and temper at 900°F	110 ksi - $\sqrt{in.}$
Quench and temper at 1100°F	128 ksi - $\sqrt{in.}$

Transverse tensile specimens from the vicinity of the fracture origin indicated the following strengths, as noted in Table III.

Yield Strength = 128 ksi

Tensile Strength = 159 ksi

For a crack which is longer than it is deep, Q = 1.2. Assuming the stress level at the crack tip equals the yield strength, and substituting K_{IC} - 128 ksi - $\sqrt{in.}$ into equation (2), $a_{critical}$ = 0.31. For K_{IC} = 110 ksi $\sqrt{in.}$, $a_{critical}$ = 0.23-inches. Both of these estimates of the critical crack depth compare favorably with the observed value of 0.25-inches. Hence, analysis via the brittle fracture theory of Tiffany and Masters suggests an initially brittle fracture. This view is consistent with the macroscopically flat fracture origin.

8.3 Battelle Equation

The following fracture mechanics analysis of cylinder 9959 is based on an empirical analysis formulated by Maxey and co-workers[26-28] at Battelle Memorial Institute. This analysis was developed for ductile fracture of pipe with yield strengths from 40 to 70 ksi. It is recognized at the outset that this analysis was not formulated for higher strength materials, but a brief exploration of its applicability and predictions relative to cylinder 9959 with a yield strength of 128 ksi seems worthwhile.

Moreover, this analysis was not formulated for a part-through crack growing from the inside wall, but for a part-through crack growing from the oustide wall. For this reason, this brief analysis will be confined to the through-wall crack in cylinder 9959 which extended as flat fracture over a few inches longitudinally to either side of the fracture origin, as shown in Figure 7c. Beyond this region, slant fracture (ductile fracture) developed. It seems appropriate to apply this ductile fracture analysis in this region.

As a starting point, it is noted that stress magnification will occur at the ends of a crack. Consequently, plastic flow and fracture can occur at nominal wall stresses lower than the yield strength. In the case of a longitudinal sidewall crack in a cylinder, stress magnification is due to redistribution of the hoop stress around the crack and to bending moments caused by bulging near the crack.

The stress magnification factor due to bulging of tubular products containing a through-wall, longitudinal defect, M_T, was developed by Folias and is given by

$$M_T = (1 + 1.255 \frac{c^2}{RT} - 0.0135 \frac{c^4}{R^2 t^2}) \; 1/2 \qquad (3)$$

In the above equation,

d = depth of a part-through crack

2c = length of a through-wall crack

R = cylinder radius

t = wall thickness

The stress magnification factor shows up in the equations used to calculate the hoop stress at failure. Equations have been defined by Maxey[18] for two types of fractures, classified as "flow stress controlled" (plastic behavior) and "toughness controlled" (elastic-plastic behavior). Equations for both types of behavior appear below.

In the case of a through-wall, axial crack, the equation for toughness-controlled behavior, σ_T, is as follows:

$$\ell n \sec \frac{\pi}{2} (M_T \sigma_T / \sigma_f) = K_c^2 \pi / (8c\sigma_f^2) = 12E\pi(C_v/A_c)/(8c\sigma_f^2) \quad (4)$$

For a through-wall defect, the equation for flow stress controlled behavior is

$$\sigma_T^* = \sigma_f / M_T \quad (5)$$

In the above equations,

σ_T^* = hoop stress at failure for flow stress controlled behavior

σ_f = the flow stress of the steel (assumed by Maxey and others to be yield strength + 10,000 psi)

K_c = plane stress fracture toughness of material

C_V/A_C = impact energy in foot-lbs. per unit area of a Charpy test specimen (half size or full size)

E = Young's modulus (30×10^6 psi)

2_c = the length of the crack

M_T = stress magnification factor given by Equation 3.

Suitable analysis of equations 4 and 5 leads to the family of parametric curves plotted in Figure 27. Taking the energy for a full-size transverse Charpy specimen from near the fracture origin as 10 foot-pounds

from Table IV, and the yield strength for a transverse tensile specimen from near the fracture origin as 128 ksi from Table III gives a value for the toughness parameter on the right hand side of Figure 27 of

$$\frac{12C_v E}{A_c \sigma_f^2 \sqrt{RT}} = \frac{12(10)(30 \times 10^6)}{(0.124)(128{,}000 + 10{,}000)^2 \sqrt{(11)(1/2)}} = 0.68$$

The hoop stress at the moment of burst, σ_T, is estimated from $\sigma_T = \frac{PR}{t} = \frac{(2500)(11)}{(1/2)} = 55{,}000$ psi. Hence, $\frac{\sigma_T}{\sigma_f} = \frac{55{,}000}{138{,}000} = 0.40$.

From these two parameters, 0.68 and 0.40, a point can be located on Figure 27 as shown, thus leading to an estimate of $\frac{2c}{\sqrt{RT}} = 1.4$. This gives a value for the critical crack length of $2c = 1.4 \sqrt{(11)(1/2)} = 3.3$-inches. Reference to Figure 7a indicates that the transition from flat fracture to slant fracture began when the flat region was about 3-inches long. Hence, the empirical analysis formulated by Maxey and co-workers[26-28] predicts a result which is consistent with the observations. It may be concluded that the sidewall opened up via a flat fracture which became slant fracture after a short extension. The time frame for the extension of the flat fracture is uncertain. It may have been a few milliseconds or even a few seconds.

9. DISCUSSION

Results presented in this report lead to the conclusion that cylinder 9959 ruptured due to environmentally-assisted cracking*, as evidenced by a well-defined fracture origin which intersected the inside wall, several other cracks near the fracture origin, indications of hydrogen sulfide in the compressed gas, and evidence of sulfur near and on the fracture origin. The combination of highly susceptible steel and a high concentration of hydrogen sulfide is the probable cause of the rupture of this new cylinder in about a week. Less susceptible steel and/or a lower concentration of hydrogen sulfide would have prolonged the service life of cylinder 9959. However, the combination of a high concentration of a harmful chemical species in the product being shipped and the high allowable tensile strength, 155,000 psi, of steel used under Specification DOT 3T would probably have eventually led to rupture of a cylinder on one of the tube trailers.

Ruptures of a similar nature in compressed gas containers were reported in England in 1947.[30] Low alloy steel cylinders (nickel-chromium-molybdenum, and manganese-molybdenum) in the hardened and tempered condition had tensile strengths around 130,000 to 140,000 psi. These steels exhibited environmentally-assisted cracking at applied stresses as low as 20,000 psi in hydrogen sulfide.

---

*Environmentally-assisted cracking is mechanical metallurgy terminology for crack growth via interaction between one or more harmful chemical species and stressed steel at the crack tip. Some researchers distinguish between hydrogen-assisted cracking and other stress corrosion processes involving chemical species other than hydrogen.

The general impression from the results appearing in Section 3 is that cylinder 9959 was a marginal cylinder, in terms of its tensile and Charpy properties, and in terms of its wall thickness. The inside wall near the fracture origin showed numerous grinding marks, indicating that this region drew attention at the time of inspection. Severe banding and high hardness microzones in the microstructure close to the fracture origin were further evidence of an undesirable metallurgical conditio which promoted susceptibility to environmentally-assisted cracking. A comparison of mechanical properties test results among pieces from cylinder 9959 (tensile, Charpy, hardness) indicated noteworthy material variability, with the highest strength and hardness, and lowest toughness occurring in test specimens taken from piece RR-12. Material variability in cylinder 9959 is also suggested by the frequent transitions between slant and flat fracture observed along the entire fracture surface, as noted in Section 4.2. Results of drop weight tear tests carried out at Battelle Memorial Institute also suggest significant material variability in cylinder 9959.[5]

The concentration of hydrogen sulfide in the natural gas was more than sufficient to promote environmentally-assisted cracking in a steel with a tensile strength upwards of 150 ksi, according to guidelines published by the National Association of Corrosion Engineers.[13] The primary uncertainty about the environmentally-assisted cracking process is the time required for cracks to grow to the critical size for catastrophic rupture, which was calculated to be about 0.2 to 0.3-inches deep. Estimates of K_{ISCC} indicated that the critical crack size for hydrogen assisted growth was less than 0.1-inches deep. Several blister cracks near the fracture origin and close to the inside wall provided evidence of hydrogen

assisted cracking. Once cracks had penetrated the inside wall, any other harmful chemical species in the natural gas may have assisted in the crack growth process.

The fracture mechanics analyses in Sections 8.2 and 8.3 indicate that cylinder 9959 probably ruptured initially under plane strain conditions, with a K_{IC} value between 110 and 128 ksi-$\sqrt{in.}$. A through-wall flat fracture about 3-inches long resulted, then a fast-running shear fracture developed. The transition to shear fracture indicated a change from plane strain to plane stress conditions, which might have occurred due to lessened constraint from the cylindrical structure when the through-wall defect developed. A plane stress value of fracture toughness was estimated from the Battelle correlation,[28]

$$K_c^2 = \frac{12 C_v E}{A_c} = \frac{(12)(10)(30 \times 10^6)}{(0.394)(0.315)} , \qquad (6)$$

giving K_c = 170 ksi-$\sqrt{in.}$. The occurrence of the fast running shear fracture indicates that 170 ksi-$\sqrt{in.}$ was insufficient fracture toughness to contain a 3-inch long, through-wall flaw. Therefore, the critical defect size for catastrophic ductile fracture was less than 3-inches for the prevailing stress conditions.

10. CONCLUSIONS

1. The evidence gathered in this investigation strongly suggests that cylinder 9959 ruptured due to environmentally-assisted cracking.
2. Cylinder 9959 was new and ruptured after about a week in natural gas service. Rupture in this short time was probably due to the combination of highly susceptible steel and a high concentration of hydrogen sulfide.
3. Cylinder 9959 appeared to be a marginal cylinder in terms of its tensile and Charpy properties, and in terms of its wall thickness. Generally, the wall thicknesses are less than these appearing in the inspector's report. Charpy and tensile properties were variable, and in some locations in cylinder 9959, did not meet the specification requirements. Limited tensile data obtained on steel from another 3T cylinder did meet specification requirements.
4. Metallurgical banding was observed in steel from cylinder 9959 and from cylinder 10041. In both cases, the banding was close to the inside wall of the cylinder. Subsurface cracking occurred in banded regions of piece 12 of cylinder 9959 and was detected in transverse sections of metallographic specimens. Subsurface cracking was not detected elsewhere in cylinder 9959 or in pieces examined from cylinder 10041. It is likely that the higher hardness in the banded regions in piece RR-12 led to a higher susceptibility to subsurface cracking in these regions of piece RR-12 than in other regions of cylinders 9959 and 10041.
5. To deal with environmentally-assisted crack growth problems in the future, it appears necessary to develop a data base from which to

make decisions about tolerable combinations of:

1) strength and hardness of steel, and

2) concentrations of various harmful chemical species.

11. ACKNOWLEDGEMENTS

Numerous NBS staff workers contributed to the contents of this report. Outstanding metallographic work was carried out by Mr. Charles Brady. Mr. Dave Ballard assisted in scanning electron microscopy work and contributed significantly to the interpretation of scanning electron microscope fractographs. Mr. Len Smith assisted in mechanical testing, photographic work and report assembly. Mr. George Hicho performed the K_{ISCC} tests, and Mr. Don Harne performed the Charpy tests. Mr. Dale Newbury and Mr. Chuck Fiore carried out the electron microprobe work. Dr. E. Passaglia provided valuable contributions to the review of this report.

Mr. Tom Groeneveld and Mr. William Maxey of Battelle Memorial Institute made significant contributions to developing findings about cylinder 9959 and interpreting them.

Mr. A. Mallen, Mr. J. Jones and Mr. J. Osteen of OHMR-MTB-DOT made significant contributions to the planning and implementation of this investigation. Mr. Mallen and Mr. Osteen provided valuable contributions to the review of this report.

Mr. Maurice Bolinger, Jr., Mr. Roger McCombs, and Mr. William Tholke of Gladstone Laboratories provided valuable assistance in analysis of the incident site, and in obtaining material from cylinder 9959 for analysis. They also provided useful tensile and metallographic data and photographic documentation.

Mr. Gobel Mattingly of Compressed Gas Corporation provided valuable assistance in analysis of the incident site and in the matter of gas sampling.

Messrs. Al Weber, John Nasci, Robert Schell, Herb Phelps, Alex Loginow, Ray McCartney, William Forgeng, Jr., and John Gilligan of U.S. Steel Corporation provided valuable commentary and assistance throughout the course of this investigation.

Messrs. Steve Wechter, Frank Kramer and Woody Sarrow of Airco Industrial Gases were extremely cooperative, skilled and dedicated in carrying out the gas analyses reported in Section 6.

12. BIBLIOGRAPHY

1. Code of Federal Regulations, Title 49, Transportation p. 657,1977. U.S. Government Printing Office, Washington, D.C. 20402.

2. Report of Inspection of Gas Cylinders, July 6, 1977-Original Date/ July 25, 1977--Revision Date. Robert W. Hunt Company, Engineers, 810 South Clinton Street, Chicago, Illinois 60607.

3. "Pressure-Testing Relief Valves," Correspondence Dated November 21, 1977 from C. A. Robinson, Robinson Engineering, 4920 Bellemeade Avenue, Evansville, Indianna, 47715 to Mr. Gilbert M. Ellis, Assistant State Fire Marshall, Department of Housing, Buildings and Construction, Frankfort, Kentucky 40601.

4. Progress Reports from Bruce W. Christ, National Bureau of Standards, to Arthur J. Mallen, OHMR-DOT.

   a. January 5, 1978 "Pneumatic Burst of 3T Trailer Tube No. 9959.

   b. January 10, 1978 "Visit to Gladstone Laboratory, Cincinnati, Ohio, To Survey Pieces of Burst 3T-Tube 9959".

   c. April 14, 1978 "Susceptibility of Steels Used for Compressed Gas Containers to Sustained Load Environmental Cracking."

   d. April 13, 1978 "Gas Analysis-Hydrogen Sulfide Samples Taken from Two Natural Gas Wells in the Shrewsbury Field Near Litchfield, Kentucky.

   e. June 8, 1978 "Determining Effects of Harmful Chemical Species in DOT Specification 3T Trailer Tubes (Seamless Pressure Vessels for Over-The-Highway Use).

   f. July 6, 1978 "Technical Feasibility of Shipping Natural Gas in Steel DOT Specification Compressed Gas Containers."

   g. July 19, 1978 "Specimen for Electron Microprobe Analysis from Ruptured 3T Trailer Tube 9959."

5. W. A. Maxey and T. P. Groeneveld: "Evaluation of the Use of DOT Type 3T Cylinders for the Transportation of Natural Gas", Report Issued to the Goodyear Tire and Rubber Company, Sept. 1, 1978, From Battelle-Columbus Laboratories, Columbus, Ohio.

6. American Iron and Steel Institute (AISI) Steel Products Manual. "Alloy Steel: Semifinished; Hot Rolled and Cold Finished Bars", AISI, Washington, D.C., August, 1970.

7. a. J. R. Low, D. F. Stein, A. M. Turkalo and R. P. Laforce: Transactions of the Metallurgical Society of AIME, 1968, vol. 242, p. 14.

b. C. J. McMahon, Jr.: Temper Embrittlement in Steel, ASTM STP 407, pp. 127-67, ASTM, Phila., PA. 1968.

c. K. Yoshino and C. J. McMahon, Jr.: Transactions of the Metallurgical Society of AIME, 1974, vol. 5, p. 363.

8. R. M. Brick and A. Phillips: Structure and Properties of Alloys, pp. 65-68. McGraw-Hill Book Company, Inc., New York, 1949.

9. B. F. Brown, Stress Corrosion Cracking Control Measures, National Bureau of Standards Monograph 156, U.S. Government Printing Office, Washington, D.C., 1977.

10. C. A. Zapffe and C. E. Sims: "Hydrogen Embrittlement, Internal Stress and Defects in Steel", paper reproduced on pp. 13-59 of Hydrogen Damage, edited by C. D. Beachem, Published by American Society for Metals, Metals Park, Ohio 44073, (1977).

11. "Corrosion of Oil and Gas Well Equipment", Book 2, American Petroleum Institute, Division of Production, Dallas, Texas.

12. L. S. Darken and R. W. Gurry: Physical Chemistry of Metals, pp. 445-450. McGraw-Hill Book Company, Inc. New York, 1953.

13. NACE Standard MR-01-75 (1978 Revision), "Material Requirement-Sulfide Stress Cracking Resistant Metallic Materials for Oil Field Equipment", National Association of Corrosion Engineers, P. O. Box 986, Katy, Texas 77450.

14. NACE Task Group T-IF-9, "Specification for A Standard Sulfide Corrosion Cracking Test", Draft Document Being Prepared. National Association of Corrosion Engineers, P. O. Box 986, Katy, Texas 77450.

15. S. T. Rolfe and J. H. Barsom: Fracture and Fatigue Control in Structures, Applications of Fracture Mechanics, p. 300. Prentice-Hall, Inc., Englewood Cliffs, New Jersey.

16. ASTM E 399-72, "Standard Method of Test for Plane Strain Fracture Toughness of Metallic Materials", American Society for Testing and Materials, 1916 Race Street, Philadelphia, PA 19103.

16a. J. A. Bennett and H. Mindlin: "Metallurgical Aspects of the Failure of the Point Pleasant Bridge", ASTM Journal of Testing and Evaluation, Vol. 1, No. 2, p. 152, 1973.

17. Gas Quality Laboratory Test Reports. Suction of Compressor, RENFRO #1, RENFRO #3, Robinson Engineering, 4920 Bellemeade Ave., Evansville, Indianna, 10/27/77.

18. Mr. S. Wechter: Airco Industrial Gases, Riverton, New Jersey 08077.

19. B. J. Moore: U. S. Bureau of Mines Circular 8749, "Analysis of Natural Gases, 1976", U.S. Government Printing Office, Washington, D.C. 20402.

20. W. G. Clark, Jr., "Stress Corrosion Crack Initiation in High Strength Type 4340 Steel", Flaw Growth and Fracture, ASTM STP 631, pp. 121-138, American Society for Testing and Materials, Philadelphia, PA, 1977.

21. ASTM D1143-63, "Standard Test Method for Water Vapor Content of Gaseous Fuels by Measurementof Dew-Point Temperature", Part 5.3, American Society for Testing and Materials, 1916 Race St., Philadelphia, PA 19103.

22. A. Brown, J. T. Harrison and R. Wilkins: "Electrochemical Investigations of Stress Corrosion Cracking of Plain Carbon Steel in the Carbon Dioxide-Carbon Monoxide-Water System", p. 686, Stress Corrosion Cracking and Hydrogen Embrittlement of Iron Base Alloys, National Association of Corrosion Engineers, 1440 South Creek, Houston, Texas 77084, 1977.

23. M. Kowama and S. Nagata: "Stress Corrosion Cracking of Mild and Low Alloy Steels in CO-CO_2-H_2O", p. 680, Stress Corrosion Cracking and Hydrogen Embrittlement of Iron Base Alloys, National Association of Corrosion Engineers, 1440 Southcreek, Houston, Texas 77084, 1977.

24. C. J. Tiffany and J. N. Masters: "Applied Fracture Mechanics", Fracture Toughness Testing and its Applications, ASTM STP 381, pp. 249-278, American Society for Testing and Materials, Philadelphia, PA 1965.

25. A. W. Loginow and E. H. Phelps: "Steels for Seamless Hydrogen Pressure Vessels", Paper Presented at 1974 Petroleum Mechanical Engineering Conference, Dallas, Texas, Sept., 1974, From Research Laboratory, U.S. Steel Corporation, Monroeville, PA 15146.

26. W. A. Maxey, J. F. Kiefner, R. J. Eiber and A. R. Duffy: "Ductile Fracture Initiation, Propagation, and Arrest in Cylindrical Vessels." ASTM STP 514, Fracture Toughness. ASTM, Philadelphia, PA 1972.

27. J. F. Kiefner, W. A. Maxey, R. J. Eiber and A. R. Duffy: "Failure Stress Levels of Flaws in Pressurized Cylinders." ASTM STP 536, Progress in Flaw Growth and Fracture Toughness Testing. ASTM Philadelphia, PA, 1973.

28. W. A. Maxey: "Fracture Initiation, Propagation and Arrest," pp. J-1 to J-31 in Fifth Symposium on Line Pipe Research, Houston, Nov., 1974. Pipeline Research Committee of American Gas Association, 1515 Wilson Boulevard, Arlington, VA 22209.

29. E. S. Folias: "The Stresses in a Cylindrical Shell Containing an Axial Crack," ARL 64-174, Aerospace Research Laboratories, 1964.

30. W. P. Rees: "Note on Stress Corrosion Cracking of 11021 Steels in the Presence of Sulphur Compounds," pp. 333-335, Symposium on Internal Stresses in Metals and Alloys, The Institute of Metals, 4 Grosvenor Gardens, London, S.W.1, 1948.

Table I

Chemical Composition

Element	Results From Cylinder 9959		++Requirements of Specification DOT 3T	
	National Bureau of Standards* Washington, D. C. (wt. pct.)	Gladstone Labs+ Cincinnati, Ohio (wt. pct.)	Ladle Analysis (wt. pct.)	Check Analysis (wt. pct.)
Carbon	0.44	0.42, 0.42	0.30 to 0.50	+0.04/-0.03
Manganese	0.92	0.82, 0.81	0.75 to 1.05	±0.04
Phosphorus	0.014	0.012, 0.013	0.035_{max}	+0.01
Sulfur	0.017	0.018, 0.019	0.04_{max}	+0.01
Silicon	0.27	0.20, 0.20	0.15 to 0.35	+0.03/-0.02
Chromium	0.98	0.95, 0.94	0.8 to 1.15	±0.05
Molybdenum	0.20	0.19, 0.18	0.15 to 0.25	±0.02

* Chemical analysis carried out by Chicago Spectro Laboratory, Chicago, Illinois.

\+ Chemical analysis carried out by Frank Broeman & Co., Cincinnati, Ohio.

++ Paragraph 178.45-5-(a)

Table II

Residual Element Content

Element	Results From Cylinder 9959		AISI Maximum Limits of Residual Elements (Ref. 6) (wt. pct.)
	National Bureau of Standards* Washington, D. C. (wt. pct.)	Gladstone Laboratories+ Cincinnati, Ohio (wt. pct.)	
Copper	0.01	0.015, 0.015	0.35
Nickel	0.02	0.03, 0.028	0.25
Aluminum	0.032	0.028, 0.026	++
Titanium	<0.01	0.016, 0.016	++
Nitrogen	0.0075	<0.003, <0.003	++
Oxygen	0.058	--	++
Arsenic	<0.01	--	++
Antimony	<0.005	--	++
Tin	<0.005	--	++

* Chemical analysis carried out by Chicago Spectro Laboratory, Chicago, Illinois.

\+ Chemical analysis carried out by Frank Broeman & Co., Cincinnati, Ohio.

++ Unspecified

Table III

Summary of Tensile Test Results On Specimens Taken From Cylinder 9959

Source of Data	Location of Test Specimen	Cross-Section of Test Specimen (inches)	Orientation of Test Specimen	0.2% Offset Yield Strength (psi)	Tensile Strength (psi)	Percent Elongation in Two Inches
National Bureau of Standards, Washington, D.C.	Piece RR-12	0.458 x 0.506	Transverse	132,200	159,500	14.4
		0.458 x 0.502	Longitudinal	122,700	158,600	13.6
		0.460 x 1.500*	Longitudinal	138,000	164,000	16.4
		0.450 x 1.500*	Longitudinal	137,000	165,000	16.0
	Piece RR-10E	0.470 x 1.498*	Longitudinal	128,000	153,000	19.8
		0.467 x 0.490	Longitudinal	114,600	150,300	16.4
		0.460 x 0.493	Transverse	128,300	148,100	Broke Inside gage mark
		0.460 x 0.493	Transverse	128,800	149,800	16.4
Gladstone Laboratories, Cincinnati, Ohio	Piece RR-12	0.471 x 0.500	Transverse	117,100	151,300	14.0
		0.467 x 0.504	Transverse	128,400	159,000	14.5
		0.458 x 0.493	Transverse	132,500	168,900	16.0
		0.458 x 0.501	Longitudinal	128,300	153,400	13.0
		0.461 x 0.499	Longitudinal	148,700	170,500	13.0
	Piece RR-10E	0.471 x 0.500	Transverse	109,000	136,200	16.5
		0.467 x 0.496	Transverse	109,700	139,400	16.0
		0.467 x 0.494	Longitudinal	114,200	140,000	17.5
		0.467 x 0.493	Longitudinal	116,600	136,500	14.0

* These specimens are of the same size as those used in testing by the independent inspector approved by the Department of Transportation to evaluate conformance to Specification DOT 3T.

Table IV

Summary of Charpy Test Results On Specimens Taken From Cylinder 9959
Test Temperature = 0°F Full Size Specimens

Source of Data	Location of Test Specimen	Orientation of Test Specimen	Identification Number of Test Specimen	Absorbed Energy (foot - pounds)	Lateral** Expansion (inches)	Requirements of Specification DOT 3T Sub-Paragraph 178.45-15-(a)-(3)
National Bureau of Standards Washington, D.C.	Piece RR-12	Longitudinal	18	18.5	0.008	For tests at 0°F, on full size, longitudinal Charpy specimens. Average value for acceptance for 3 specimens- 25.0 foot - pounds Minimum value 1 specimen only of the three-20.0 foot pounds
		Longitudinal	19	18.0	0.010	
		Longitudinal	101	19.5	0.015	
		Transverse*	15	10.0	0.008	
		Transverse*	16	10.5	0.005	
		Transverse*	17	12.0	0.005	
	Piece RR-10E	Longitudinal	8	25.0	0.013	
		Longitudinal	9	27.5	0.020	
		Longitudinal	10	25.0	0.016	
		Transverse*	5	16.8	0.011	
		Transverse*	6	17.5	0.011	
		Transverse*	7	17.5	0.011	

* Transverse specimens are not required in Specification DOT 3T. These results are included for completeness and future reference.

** Lateral expansion is not required in Specification DOT 3T. These results are included for completeness and future reference.

Table V

Summary Of Cracks Found In Piece RR-12*

Specimen Identification	Location of Crack	Type L Cracks		-Type C Cracks- Depth Beneath Inside Wall (inches)	Remarks
		Maximum Length (inches)	Maximum Depth (inches)		
Fracture Origin	Edge of piece RR-12 (See Fig. 5)	1.3	0.25	0.08	As noted in the text, 3 closely-spaced cracks may have linked up to form the fracture origin.
1A	Edge of piece RR-12 at location TR-1 (See Fig. 7c)	Not Measured	0.097	0.032 0.121	One type L crack and two type C cracks were detected in this specimen. (See Fig. 11). The type L crack is a subsurface crack. The type C cracks occur at the ends of the type L crack.
5AR	Edge of piece RR-12 at location TR-5 (See Fig. 7c)	-	-		One type C crack was detected in this specimen. (See Fig. 16)
6A	Edge of piece RR-12 at location TR-6 (See Fig. 7c)	-	-		One type C crack was detected in this specimen. (See Fig. 12)
R	Edge of piece RR-12 at end (See Fig. 7c)	-	-		One type C crack was detected in this specimen. (See Fig. 25)
RR-12-11		0.125 (At Surface)	Not Measured		One type L crack was detected in this specimen at Gladstone Lab.
RR-12-13		0.75	0.3		One type L crack was detected in this specimen.
RR-12-14		0.09	0.115	0.015 0.115	One type L crack and two type C cracks were detected in this specimen. (Specimen examined at Battelle-Columbus)
RR-12-G		0.8 plus	0.36	Only a longitudinal section was examined	One type L crack was detected in this specimen. (Specimen examined at Battelle-Columbus)

* Except where noted otherwise, all cracks were examined at the National Bureau of Standards.

Table VI

Results* Of Electron Microprobe Analysis
Of A Banded Region in Specimen L

Element	Multiplying Factor Above Background	Background (wt. pct.) (as determined from Table I)	Estimated Concentration in Band (wt. pct.)
Phosphorus	1.5	0.014	0.021
Chromium	1.3	0.98	1.274
Molybdenum	1.3	0.20	0.26
Manganese	1.2	0.92	1.104
Silicon	1.2	0.27	0.324
Carbon	1.0	0.44	0.44
Sulfur	1.0	0.017	0.017

* These results were obtained at the U.S. Steel Applied Research Laboratory, Monroeville, PA. through arrangements made with Dr. H. Phelps.

Table VII

Microhardness Survey of Banded Regions

Specimen Identification	Location of Specimen	Hardness Inside White-Etching Microzones		Hardness Adjacent to White-Etching Microzones		Remarks
		Knoop*	Rockwell C-Scale Equivalent	Knoop*	Rockwell C-Scale Equivalent	
Fracture Origin						
1A	Edge of piece RR-12 at location TR-1 (See Fig. 7c)	443 440 440 427 425 422 453	43 43 43 42 42 41.5 44	393 412 418 402 391 393	39 40.5 40.5 40 39 39	White-etching bands were easily detected.
3A	Edge of piece RR-12 at location TR-3 (See Fig. 7c)	418 410	41 40.5	372 388 388	37 39 39	White-etching bands were easily detected.
2A	Edge of piece RR-12 at location TR-2 (See Fig. 7c)	413 416 390	41 41 39	365 390	36.5 39	White-etching bands were easily detected.
5A	Edge of piece RR-12 at location TR-5 (See Fig. 7c)	422	41.5	363 356	36 35.5	White-etching bands were easily detected.
L	Edge of piece RR-12 at end (See Fig. 7c.)		46 45		40 41 39 42	White-etching bands were easily detected. (See Fig. 25.)
R	Edge of piece RR-12 at end (See Fig. 7c)	462 410 410	44.5 41 41	352 401 376	35 40 37	White-etching bands were easily detected. (See Fig. 25)
D	Transverse section of left end of specimen labeled "D" in Fig. 5 of piece RR-12	-	-	381 378 363 366 381	38 38 36 36 38	No white-etching bands were detected.
3B	Transverse section near head of cylinder 10041 on trailer T-256 (See Fig. 6)	-	-	257 307 347 334	21 29 30 33	No white-etching bands were detected. Indentations were made in light and dark-etching bands.
5B	Transverse section near head of cylinder 10041 on trailer T-256 (See Fig. 6)	-	-	310L 292D 320L	30 27 31	No white-etching bands were detected. Indentations were made in light and dark-etching bands.
6B	Transverse section near head of cylinder 10041 on trailer T-256 (See Fig. 6)	-	-	284L 312D 330L 322L 330L	26 30 32 31 32	No white-etching bands were detected. Indentations were made in light and dark-etching bands.

* Knoop microhardness measurements were made with a 500 gram load to facilitate conversion to the Rockwell C-scale equivalent using the standard tabulation of conversions issued by the Wilson Instrument Division of American Chain & Cable Company, Inc.

Table VIII

K_{ISCC} Estimates For Steel Used In Specification DOT 3T Cylinders
(Yield Strength = 122.5 ksi Tensile Strength = 142.5 ksi)
(Steel Specimens From Cylinder 10041)

Specimen Number	Initial Stress Intensity (ksi-$\sqrt{in.}$)	Extent Of Crack Growth In Five Days Immersion[+] (inches)	Estimated K_{ISCC}[*] (ksi-$\sqrt{in.}$)	Remarks
1	35	None Detected	--	Apparently 35 Ksi-$\sqrt{in.}$ was too low to promote crack growth.
2	45	0.118	40[**]	Beyond 0.118-inches extension, the crack turned and ran across one arm of the specimen.
3	35	None Detected	--	Apparently, 35 Ksi-$\sqrt{in}$ was too low to promote crack growth.
4	45	None Detected	--	This specimen was immersed for 6 days and no crack growth was detected. It was immersed for another 5 days and still no crack growth was detected.
5	50	0.17	41.2	This specimen was entirely coated with wax except for the crack tip region, to prevent the crack from growing into an arm of the specimen.
6	49	0.212	39.2[**]	A fatigue precrack was grown at the root of the chevron in this specimen prior to immersion. Beyond 0.212-inches extension, the crack turned and ran across one arm of the specimen.

[+] This tabulation shows crack growth beyond the base of the chevron (See Fig.26).

[*] Calculated via the method reported by R.B. Heady: "Sulfide Corrosive Cracking in Gas and Oil Wells XIB," Technical Progress Report BRC-Corp 5-74-B, Shell Oil Company, Houston.

[**] Smaller K_{ISCC} values might have been determined if the crack had not turned into the specimen arm.

Table IX

Results of Hydrogen Sulfide and Moisture Analysis

Location	Hydrogen Sulfide Concentration (ppm)*	Moisture Concentration (ppm)*
Input to compressor	490 ±25	800
Gas Well-Renfro #1	603 ±25	800
Gas Well-Renfro #3	572 ±25	800

* Concentration is given in parts per million (ppm) by volume.

Table X

Results Of Gas Analysis*
(Volume Percent)

Component	Input To Compressor	Renfro #1	Renfro #3
Ethane	4.23	4.2	4.22
Propane	1.89	1.87	1.90
ISO-Butane	0.17	0.17	0.17
n-Butane	0.37	0.37	0.40
n-Pentane	0.10	0.10	0.10
Other C_5 Hydrocarbon	0.08	0.07	0.08
Nitrogen	17.0	17.6	17.6
Methane	Balance	Balance	Balance

* Hydrogen sulfide and moisture appear in Table IX.

Table XI

Results of Rockwell C-Scale Hardness
Survey On Transverse Sections

Cylinder Number	Location Along Cylinder	Specimen Identification	HRC	Remarks
9959 (Cylinder 4 on trailer T-256. See Fig. 6.)	RR 12	Specimens from 17-inch segment in Fig. 7c		These values are comparable to those found by conversion of Knoop microhardness numbers obtained outside the white-etching microzones (See Table VII.)
		TR-8	33-35	
		TR-6	31-35	
		TR-3	36	
		L	37	
		R	39	
		Specimens labeled "C" and "D" in Fig. 5		
		C	36	Measured on tensile specimen.
		D	31.6-34.5	Measured on tensile specimen.
	RR 10 (See Fig. 2)		32-35	Measured on tensile specimens.
	RR 17A (See Fig. 2)		31	Measured on tensile specimens.
10041 (Cylinder 1 on trailer T-256. See Fig. 6.)	Near front head		30.3	(Avg. of 23 indentations)
(Cylinder 9 on trailer T-254. See Fig. 1.)	Near center of sidewall at about 9 o'clock		30.0	(Avg. of 13 indentations)

Table XII

Rockwell C-Scale Hardness At Outside Surface

Cylinder	Location	Hardness At Outside Surface		
		Below Decarburized Layer (Grind Off 0.033-inches)	Just Below Paint (About 0.003-inches deep)	As-Received Surface
9959 (Cylinder 4 on trailer T-256)	RR-12	34.5	26.8	25.5
		34.0	28.2	28.5
		34.5	28.0	39.0
		34.7	28.8	27.2
		34.7	27.8	31.5
	RR-17	33.1	26.8	21.0
		33.2	26.0	24.8
		33.2	28.5	28.0
		32.8	27.5	29.3
		32.7	26.0	26.0
10041 (Cylinder 1 on trailer T-256)	Near Front Head	28.8	26.3	35.6
		28.8	26.2	39.5
		29.1	27.0	38.0
		28.2	26.5	20.0
		29.2	27.1	37.0

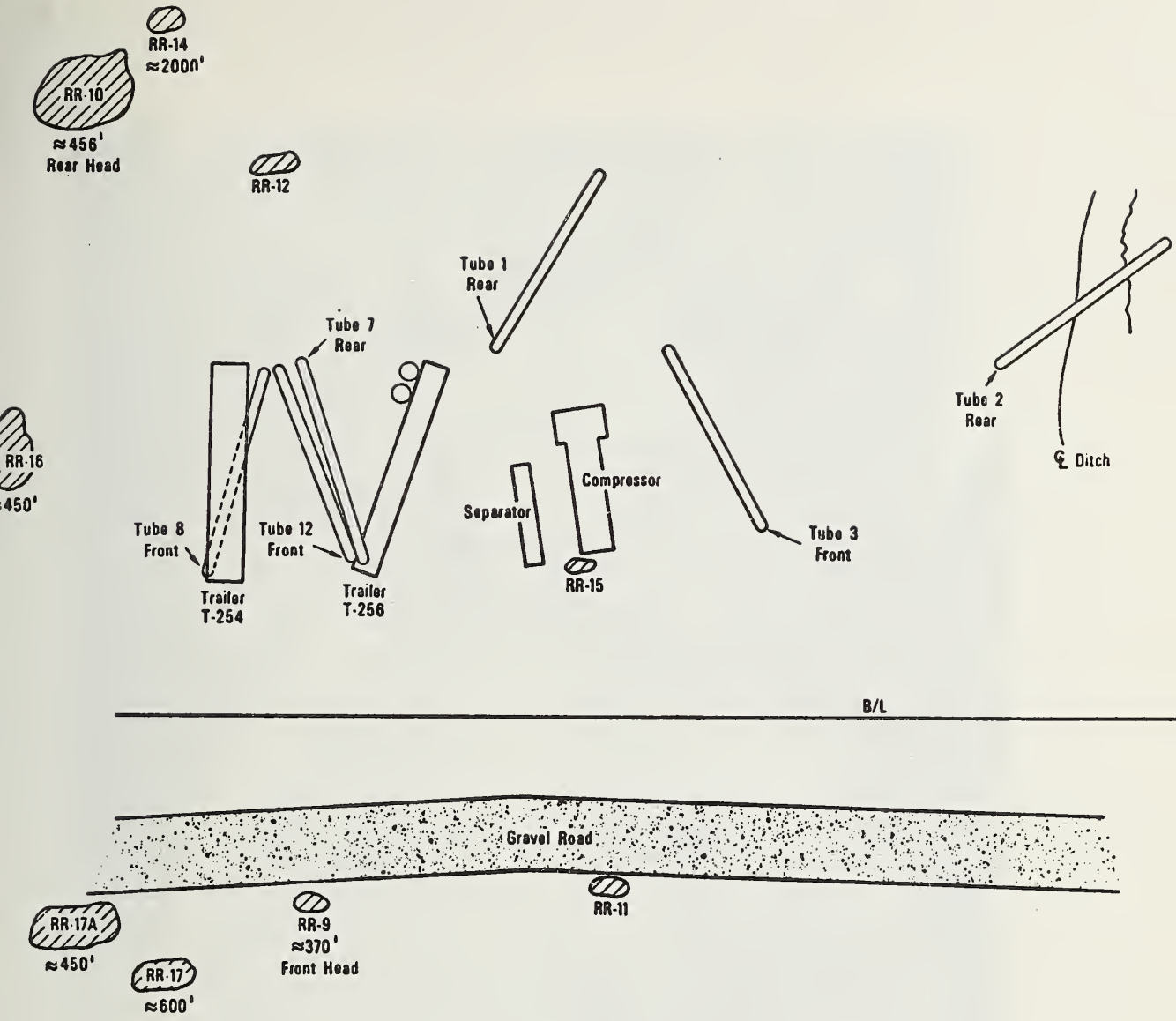

Figure 1. Incident site after the pneumatic burst. Number by each piece indicates approximate distance from remains of trailer T-256, for those pieces for which this information was provided. The relative sizes of the pieces is indicated roughly by the size in the figure. The position of each piece was indicated by Mr. Rodney Raby of the Kentucky State Fire Marshal's Office. The positions of pieces RR-18 and RR-19 were not identified.

Figure 2a. Eleven pieces of cylinder 9959 laid out on the floor at Gladstone Laboratories, Inc. The rear head is in the foreground. (Photo courtesy of M. Bolinger, Jr., Gladstone Laboratories, Inc., Cincinnati, Ohio).

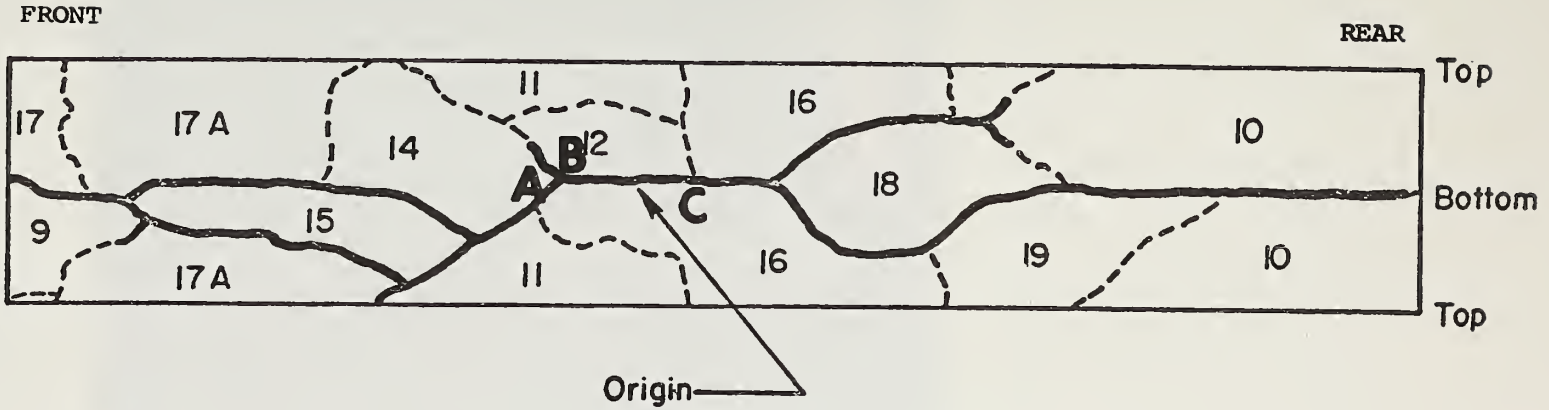

Figure 2b. Diagram of the eleven pieces of cylinder 9959, showing approximate locations of the fracture paths. The heavy black line shows the path of the primary fracture. The dashed lines indicate secondary fracture paths. (Diagram courtesy of W. Maxey, Battelle Memorial Institute, Columbus, Ohio).

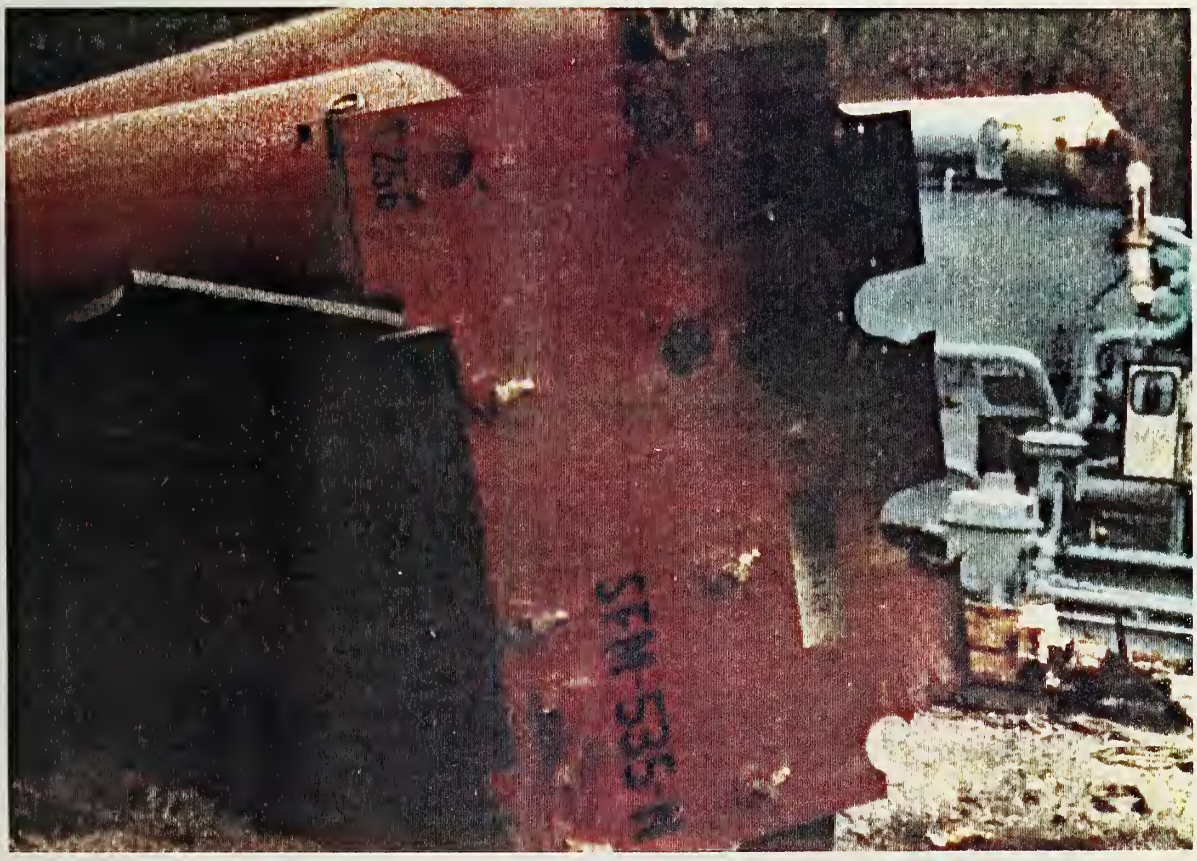

Figure 3. Remains of trailer T-256 after the incident, as seen from front. (Photo courtesy of Mr. W. Piehl, Western Sales and Testing, Inc., Amarillo, Texas.)

Figure 4. Intact tube trailer composed of specification DOT 3T cylinders. The array of cylinders on the trailer is 3-high by 4-wide. (Photo courtesy of Mr. W. Piehl, Western Sales and Testing, Inc., Amarillo, Texas.)

Figure 5. Inside wall of piece RR-12 showing location of specimen taken for chemical analysis. The arrows point in the longitudinal direction. This piece is about 30-inches wide by about 50-inches long. (Photo courtesy of M. Bolinger, Jr., Gladstone Laboratories, Inc., Cincinnati, Ohio.)

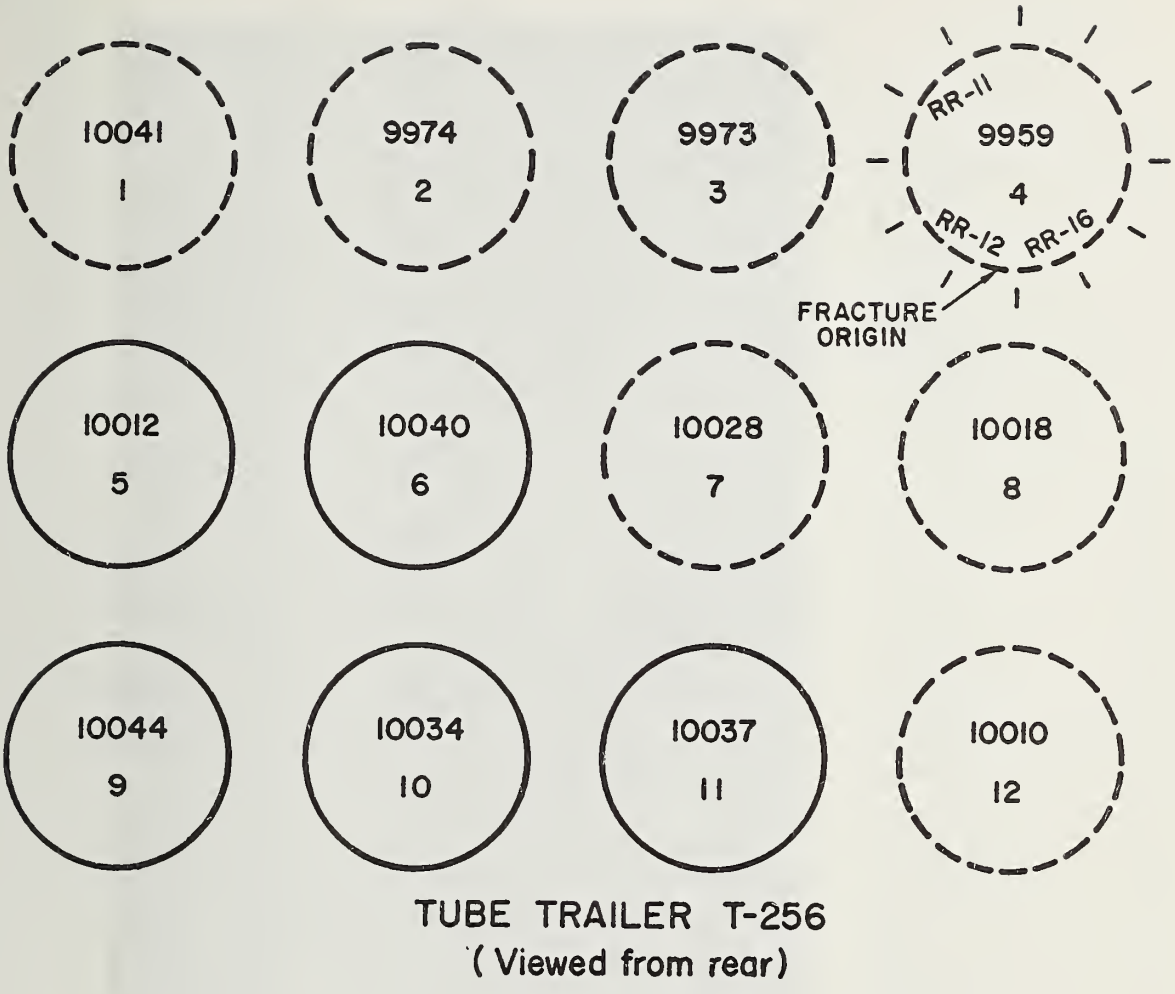

Figure 6. Array of specification DOT-3T cylinders on tube trailer T-256 as viewed from the rear. The cylinder which ruptured is on the top row at the right. The location of the fracture origin is shown. It was 12.5 feet from the front head. The "RR- " designations assigned to the pieces near the fracture origin are indicated. (Identification number for each tube supplied by Jack B. Kelly Enterprises, Inc., Amarillo, Texas.)

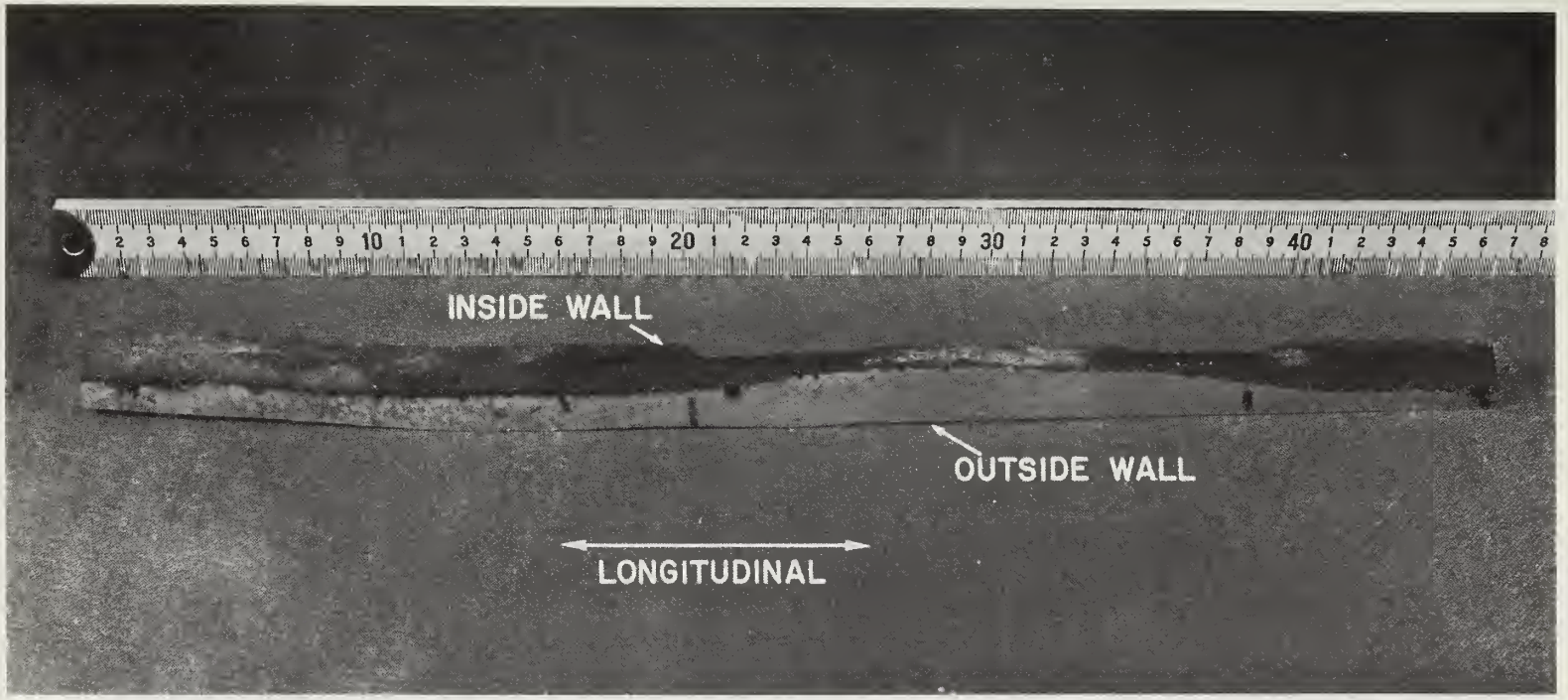

Figure 7a. Seventeen-inch long segment cut from edge of piece RR-12 along the line labeled "saw cut" in Figure 5. The scale is in centimeters. The fracture origin is opposite "31" on the scale. The transition from flat fracture to full slant fracture occurs to either side of the fracture origin, between 20 and 39 on the scale.

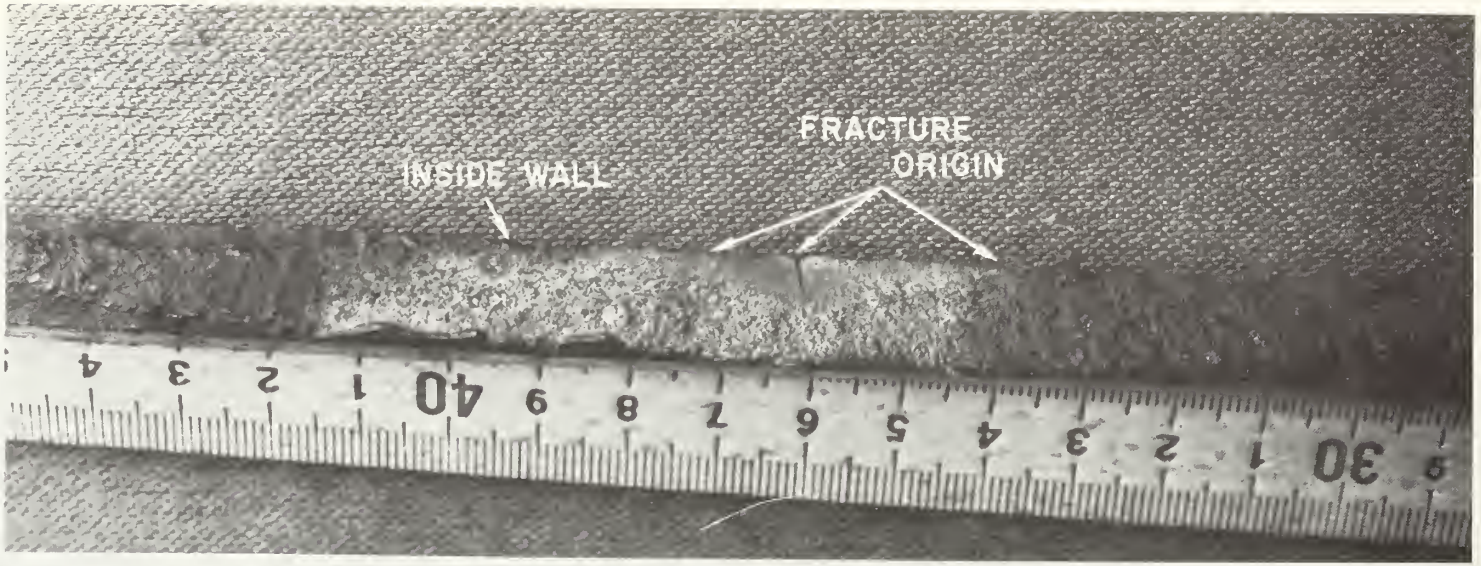

Figure 7b. View of fracture origin looking directly down on it. The scale is against the outside wall.

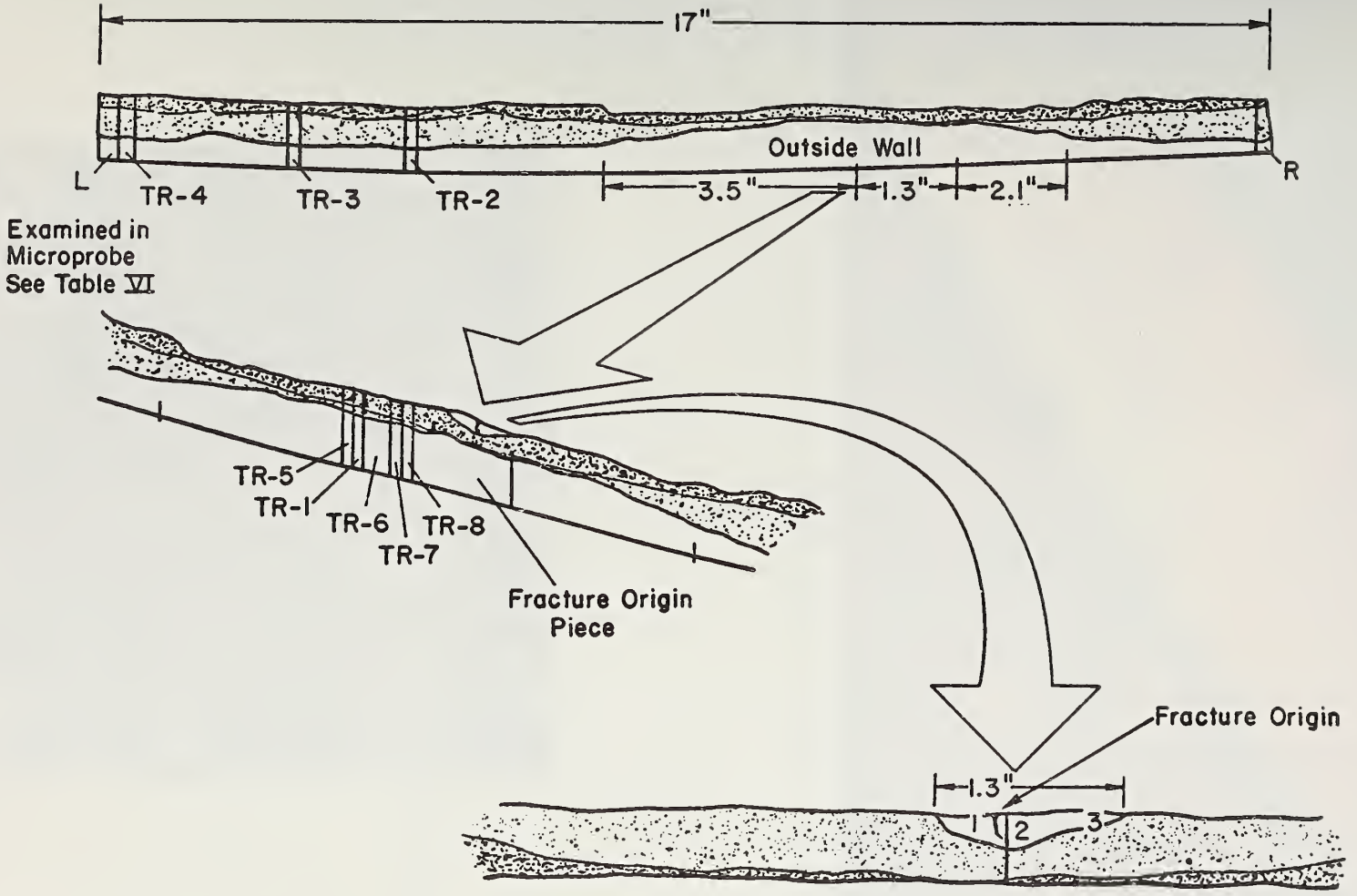

Figure 7c. Artist's drawing of the segment containing the fracture origin. Transverse sections cut from this segment are labeled "TR- ."

Figure 8a. Fracture origin on piece RR-12 before cleaning, viewed toward inside wall.

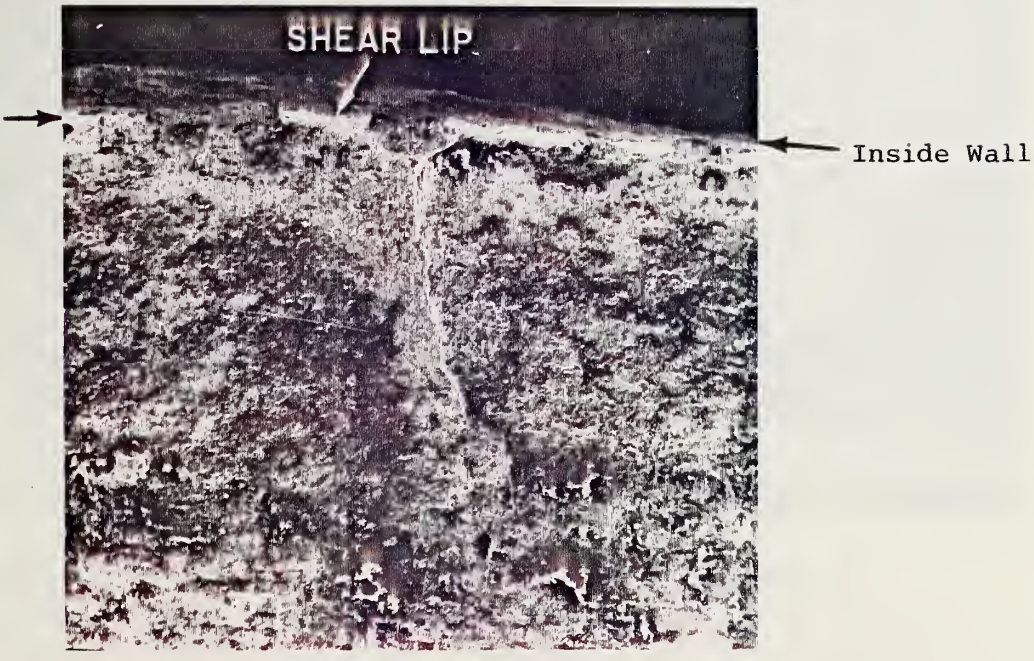

Figure 8b. Close-up view of step on fracture surface. Shear lips show up as intermittent white markings along inside wall. These shear lips are probably in the decarburized layer (see Section 5.3).

Figure 9a. Forging seams evident on inside wall at front head of cylinder 10041. The scale is in centimeters.

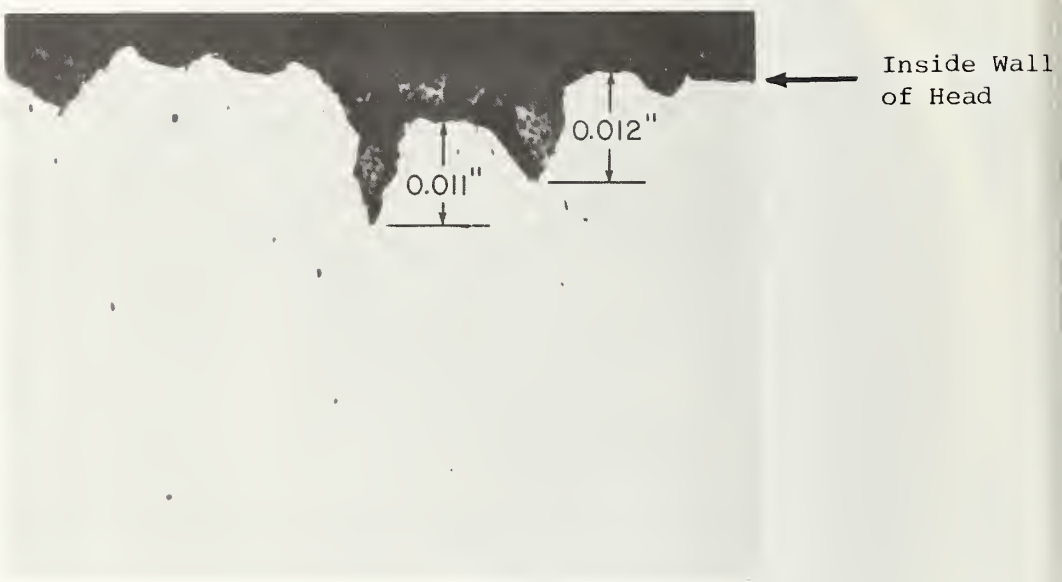

Figure 9b. Cross-section of typical forging seams found in front head of cylinder 10041.

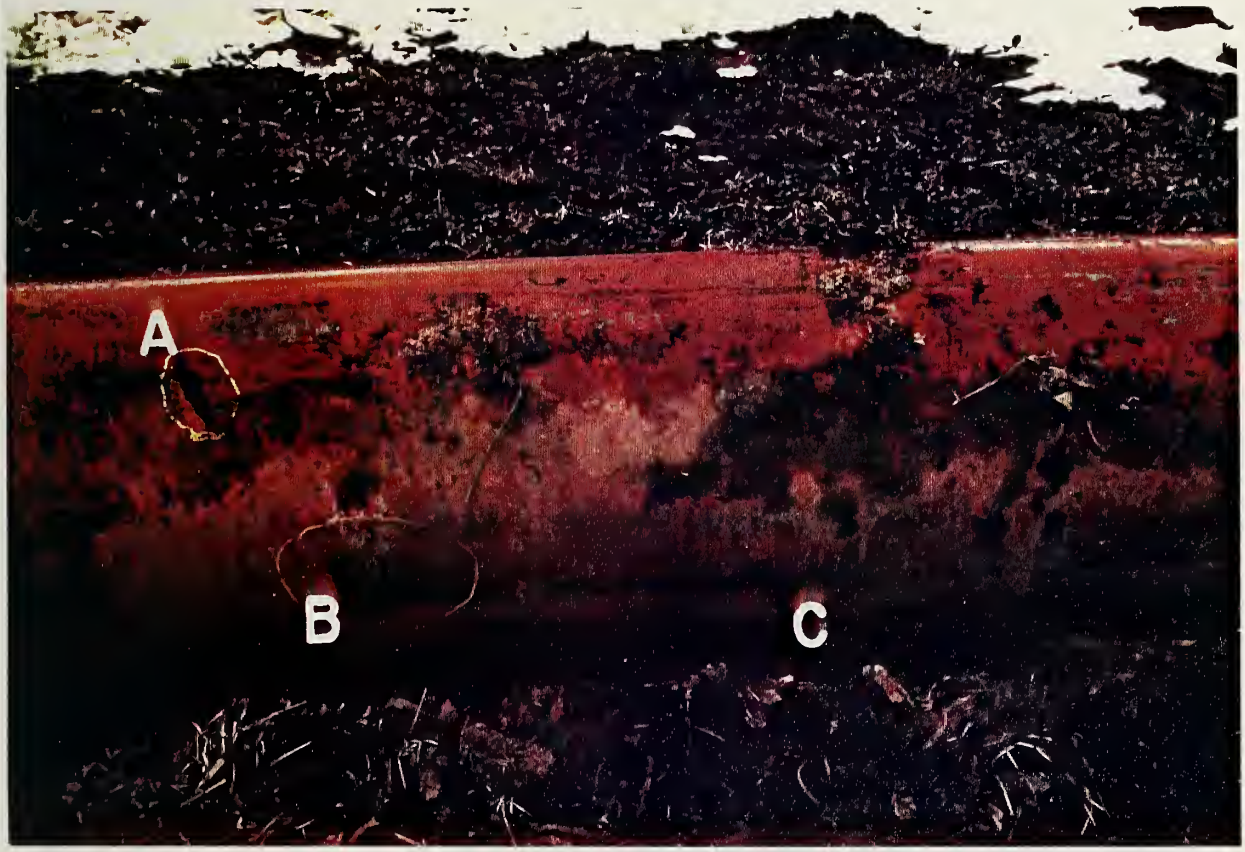

Figure 10a. Hit mark on cylinder number 8 (see Fig. 6 for location) made by opening flap of piece RR-16. The lines $\overline{AB}$ and $\overline{BC}$ in this figure correspond to the lines $\overline{AB}$ and $\overline{BC}$ in Figure 2b. The rear head of the cylinder is to the right.

Figure 10b. Bowing of cylinder Number 8 due to the blow resulting in the hit mark shown in Figure 10a.

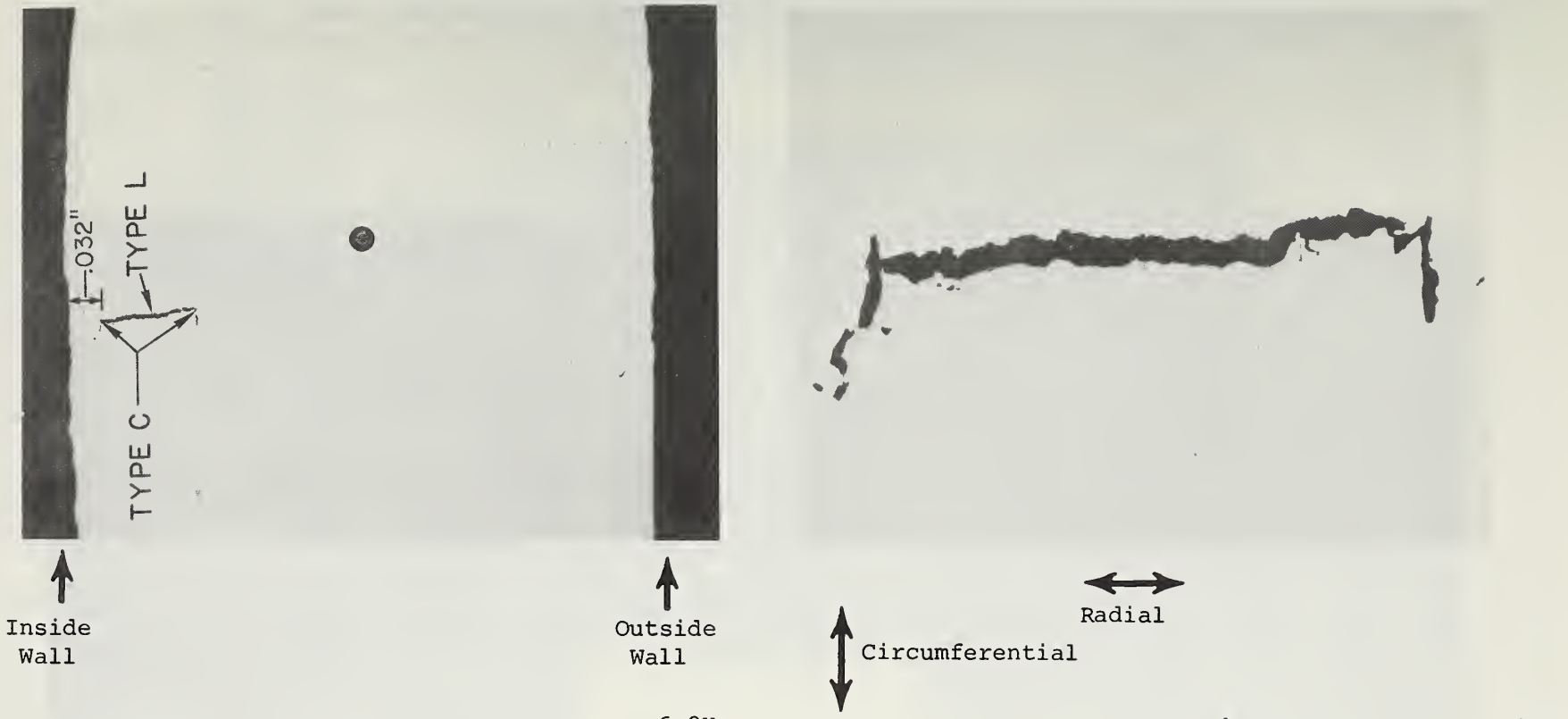

Figure 11. Type L and type C cracks detected in specimen TR-1. (See Figure 7c for specimen location.) The large black circle is a Rockwell C-scale hardness indentation. The row of tiny black dots is a series of Knoop microhardness indentations. (a) Transverse section showing full wall thickness. (b) Close-up view of the cracks.

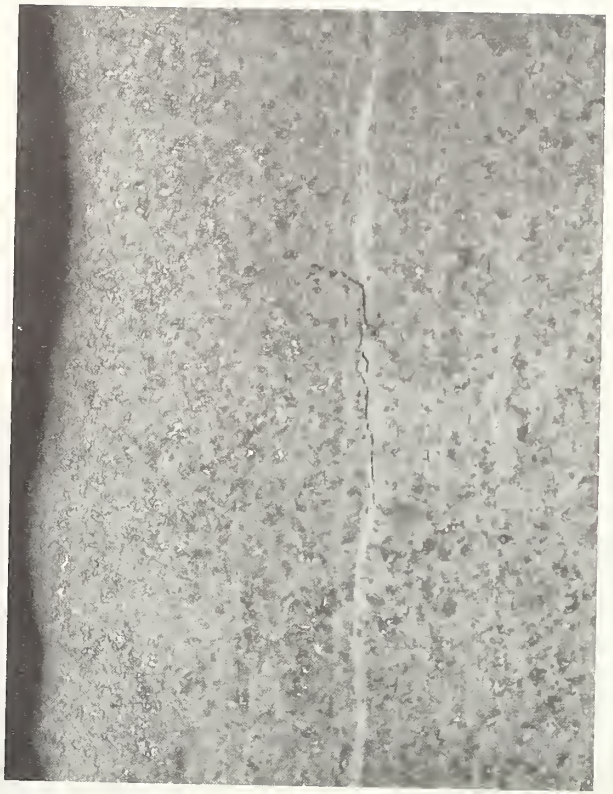

Inside Wall

a 100X
Etchant/Ammonium Molybdate.

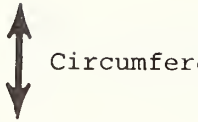

b 800X
Etchant/Ammonium Molybdate.

Figure 12. Intergranular crack path at tip of type C crack found in white-etching microzone specimen TR-6. (See Figure 7c for specimen location.) (a) Transverse section showing relationship of crack to inside wall. (b) Intergranular crack path developing at tip.

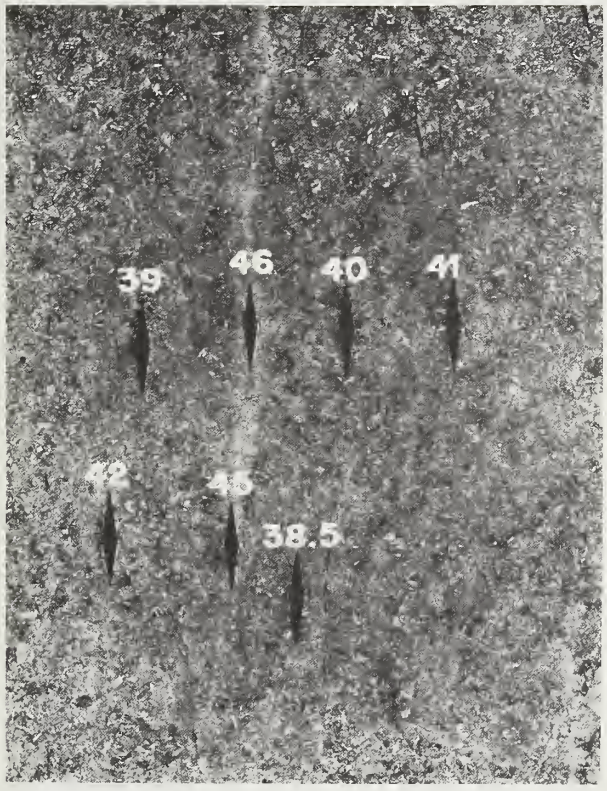

Etchant: 100X
Ammonium Molybdate

Figure 13. White-etching microzones found near inside wall in transverse specimen L. Rockwell C-scale hardness equivalents are shown. (see Figure 7c for specimen location.)

Etchant ammonium molybdate. 80X

Figure 14. Banding near inside wall detected in transverse section taken from a ring cut near the front head of cylinder 10041.

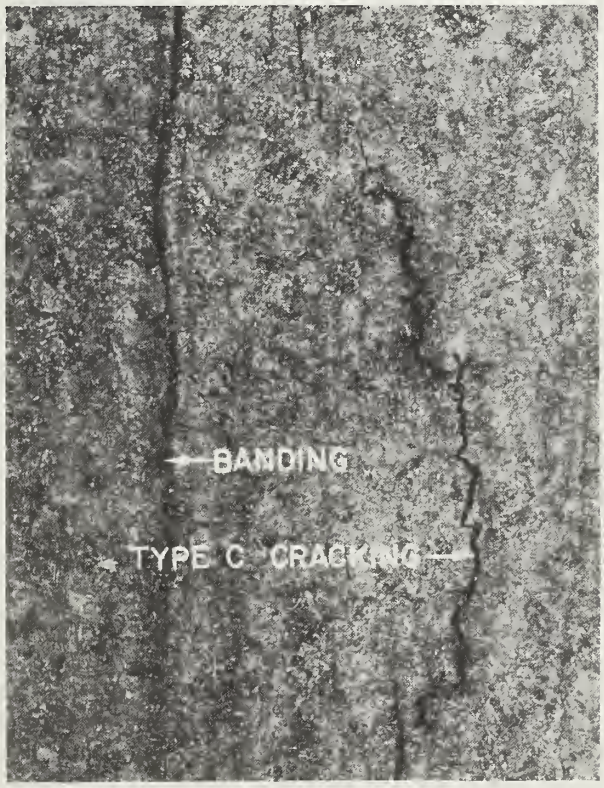

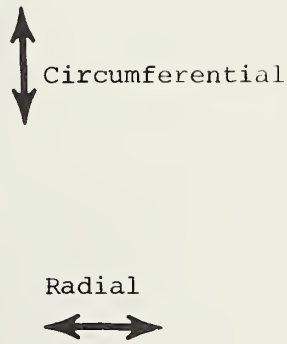

Etchant: 2% nital. 100X

Figure 15. Cracking parallel to banding and inclusions in an unstressed transverse section of a test specimen saturated with diffusible hydrogen in the laboratory. This specimen was taken from a ring cut near the front head of cylinder 10041.

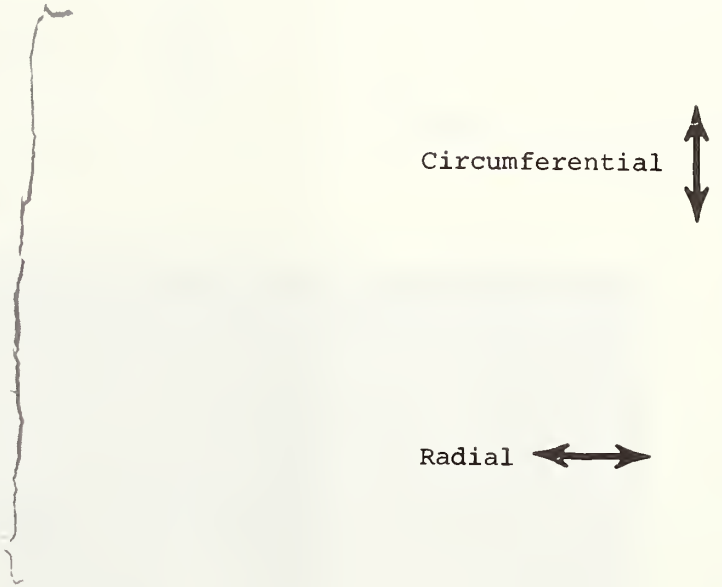

As Polished 100X
(a)

Etchant: Ammonium Molybdate 100X
(b)

Figure 16. Incipient type L cracks which appear to have originated at radial jogs in a type C crack. This cracking was found in specimen TR-5. (a) As polished section showing cracks, (b) Same section as in 16a after etching with ammonium molybdate.

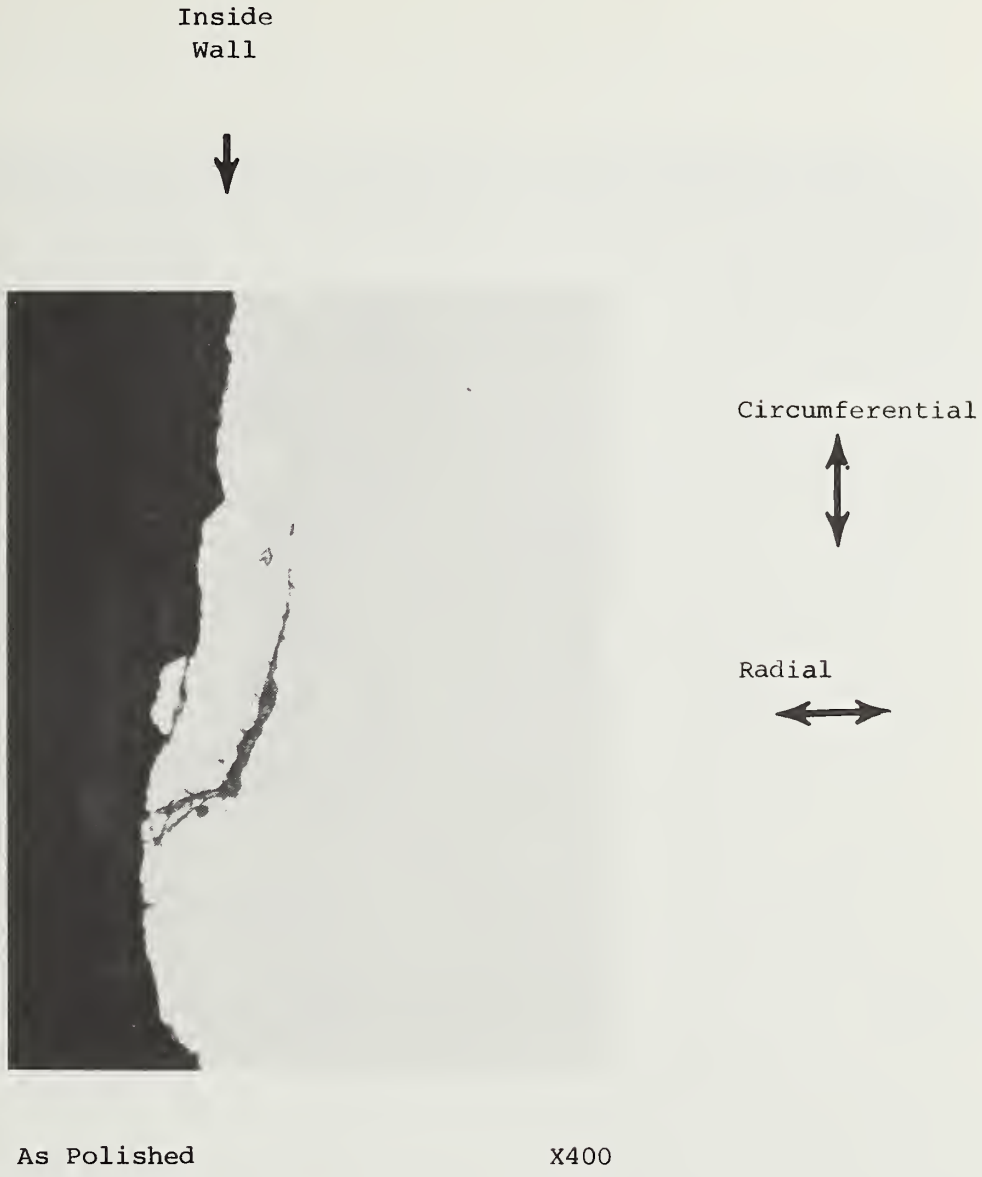

Figure 17. Surface lap detected near inside wall of cylinder 10041.

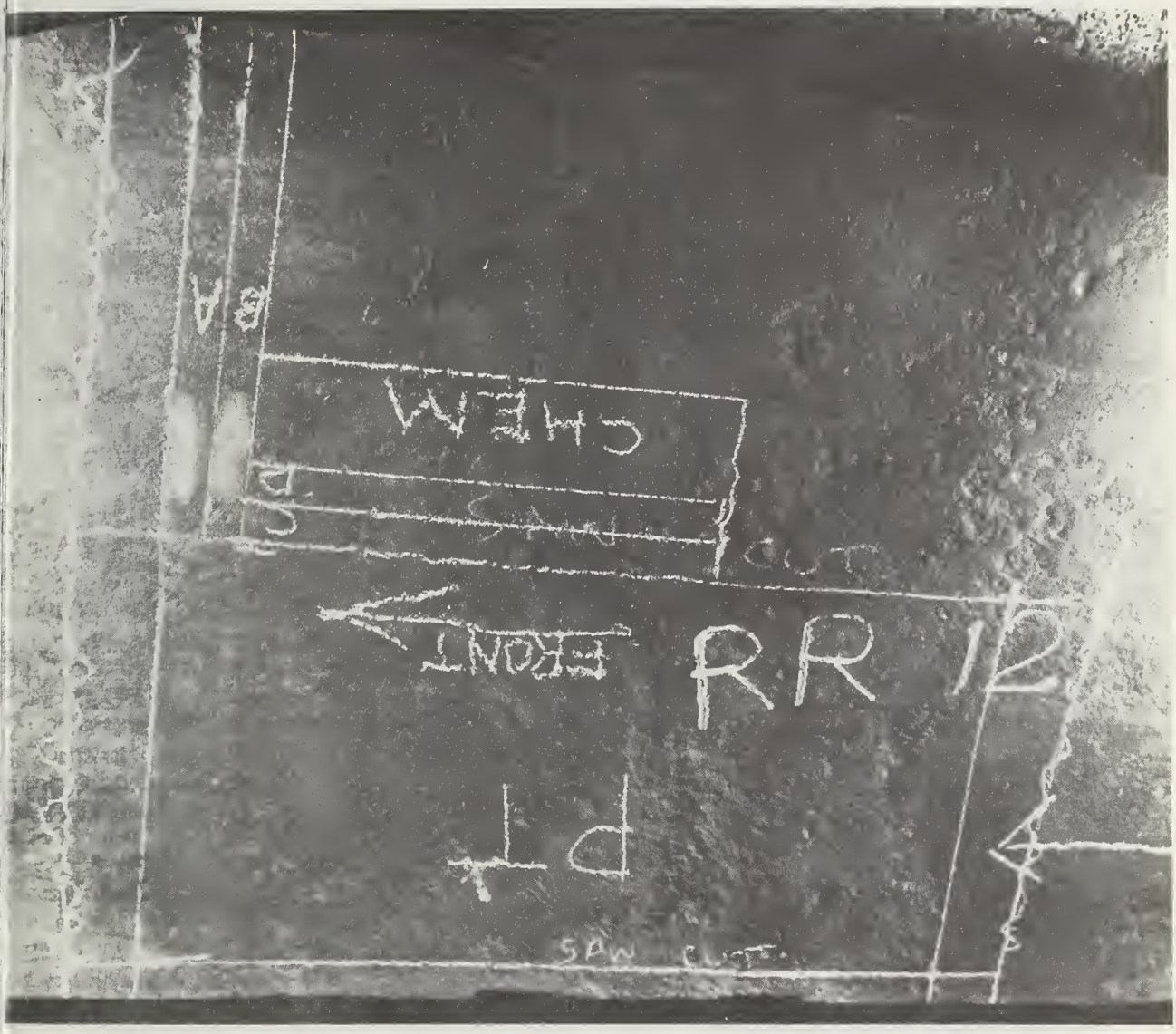

Figure 18a. A portion of piece RR-12 showing the general surface topography of the inside wall near the fracture origin. The fracture origin is along the bottom near the words "saw cut." (Photo courtesy of M. Bolinger, Jr., Gladstone Laboratories, Inc., Cincinnati, Ohio.)

Figure 18b. A view of piece RR-12 showing sets of parallel lines running in the circumferential direction. (Photo courtesy of M. Bolinger, Jr., Gladstone Laboratories, Inc., Cincinnati, Ohio.)

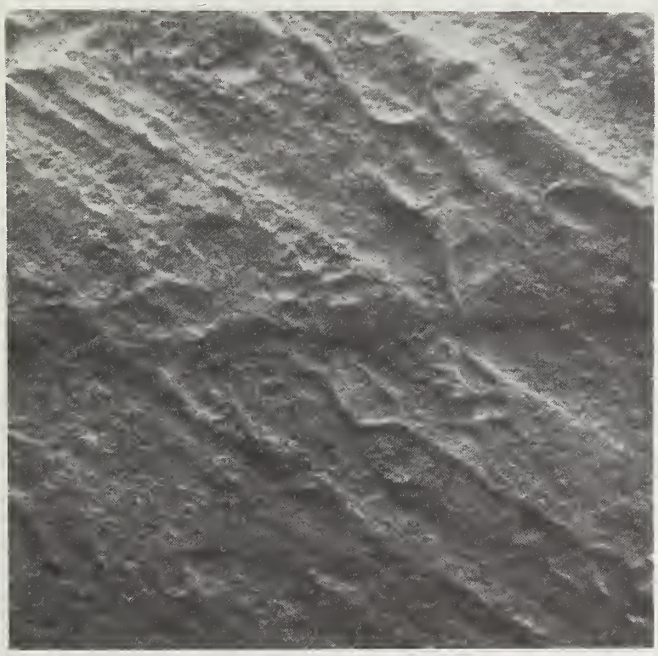

X24

Figure 19. Surface topography of the inside wall of specimen TR-1 near the fracture origin after solution cleaning, showing craters and grinding scratches. (Photo obtained in scanning electron microscope.)

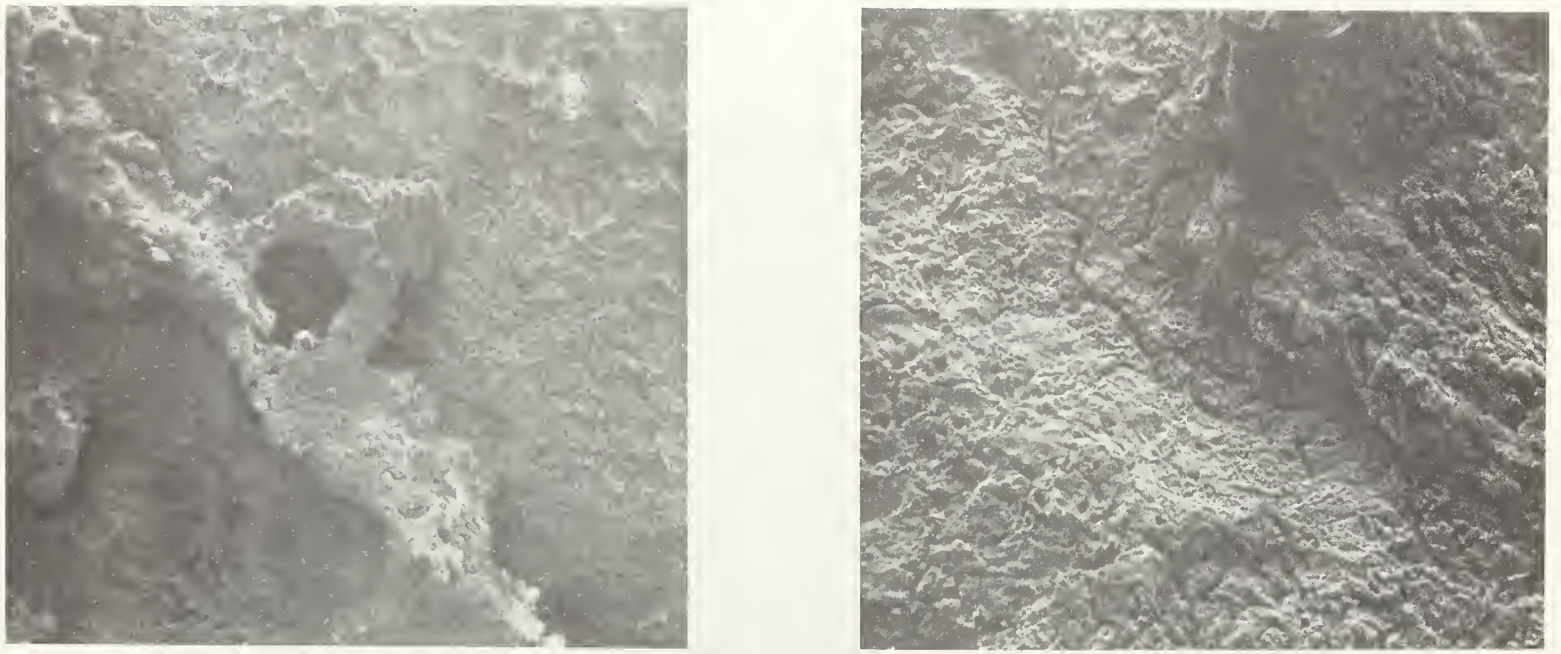

a 110X b 600X

Figure 20. The inside wall of specimen TR-5 near the fracture origin after partial solution cleaning. (a) Low magnification view of uneven regions. (Remaining surface product runs from 2 o'clock to 8 o'clock) (b) Uneven region at higher magnification. (Photo obtained in scanning electron microscope.)

Figure 21. Close-up view of the fracture origin after stripping three cellulose acetate replicas. The black product on the fracture surface became evident as the orange-brown product was stripped away. This view is towards the inside wall.

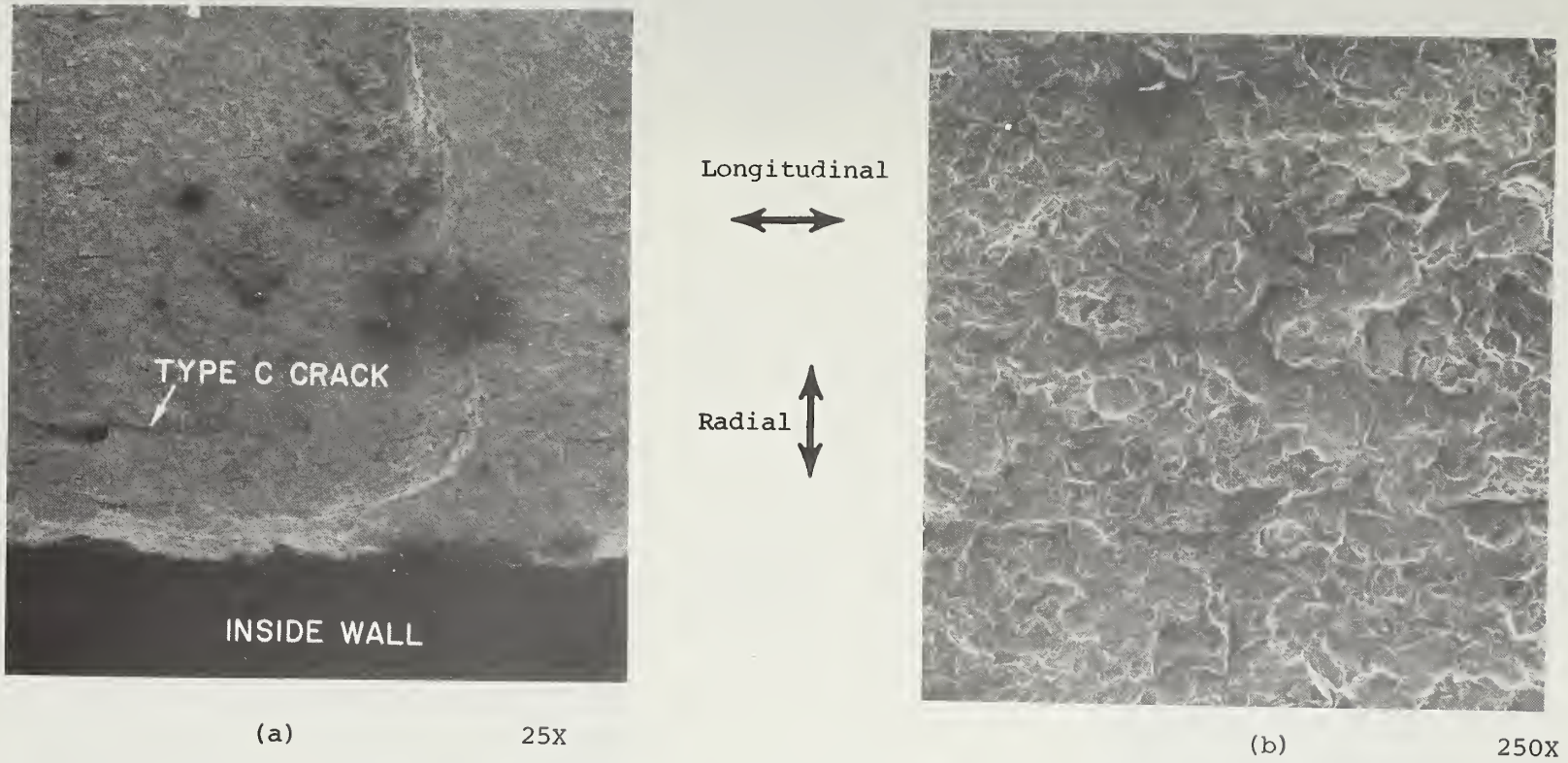

Figure 22. Scanning electron microscope views of fracture origin after cleaning with buffered HCℓ solution. (a) Region of step, showing a type C crack, (b) Region away from step, showing "plateaus and valleys" structure.

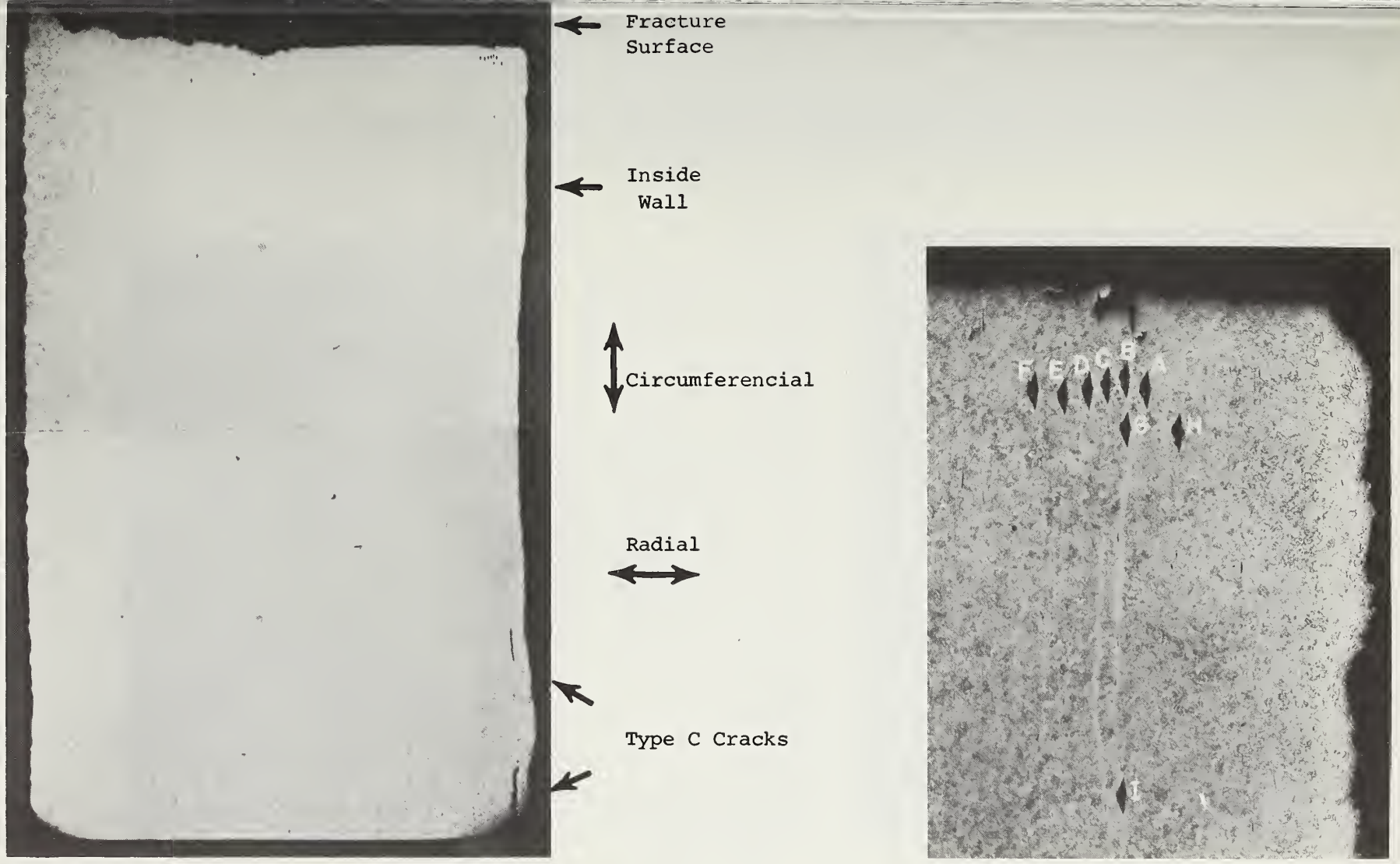

Etchant: Ammonium Molybdate 7 1/2X
(a)

Etchant: Ammonium Molybdate 50X
(b)

Figure 23. Transverse section through fracture origin. (a) Full thickness view, showing extremely flat fracture surface at origin and two type C cracks in banded region near inside wall. A 45° shear lip appears at the outside wall. (b) Close-up view of the region of the microhardness indentations at the top right in Figure 23a.

Figure 24. Typical microstructure of tempered bainite found in cylinder 9959.
Etchant: Picral 1000X

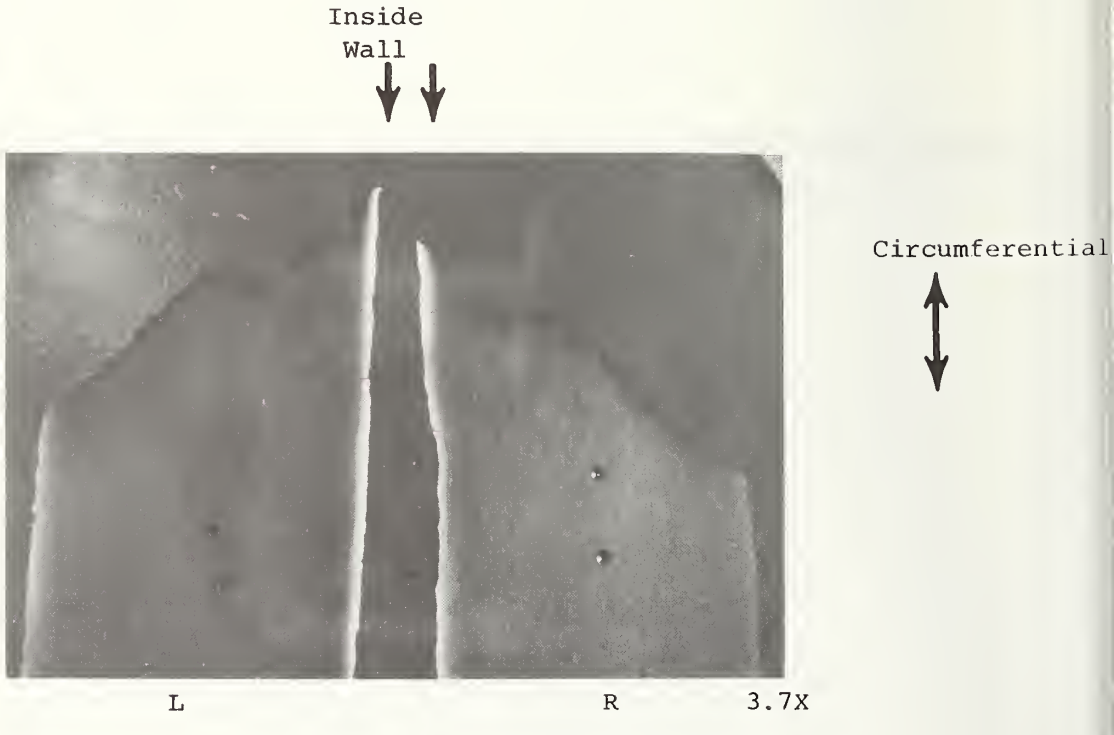

Figure 25. Transverse sections from ends of the segment from piece RR-12 shown in Figure 7c.

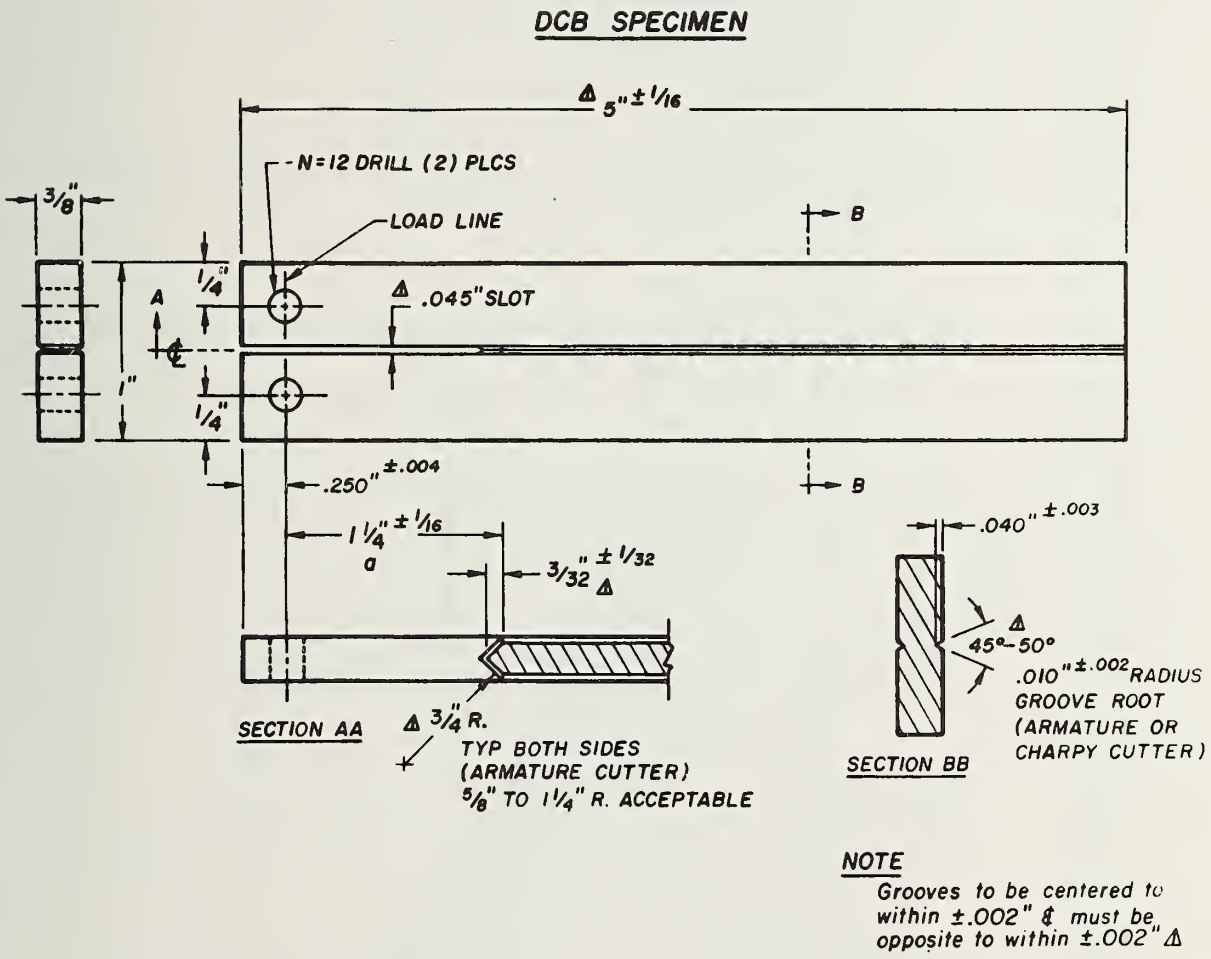

Figure 26. Diagram of the double cantilever beam test specimen used for K_{ISCC} testing.

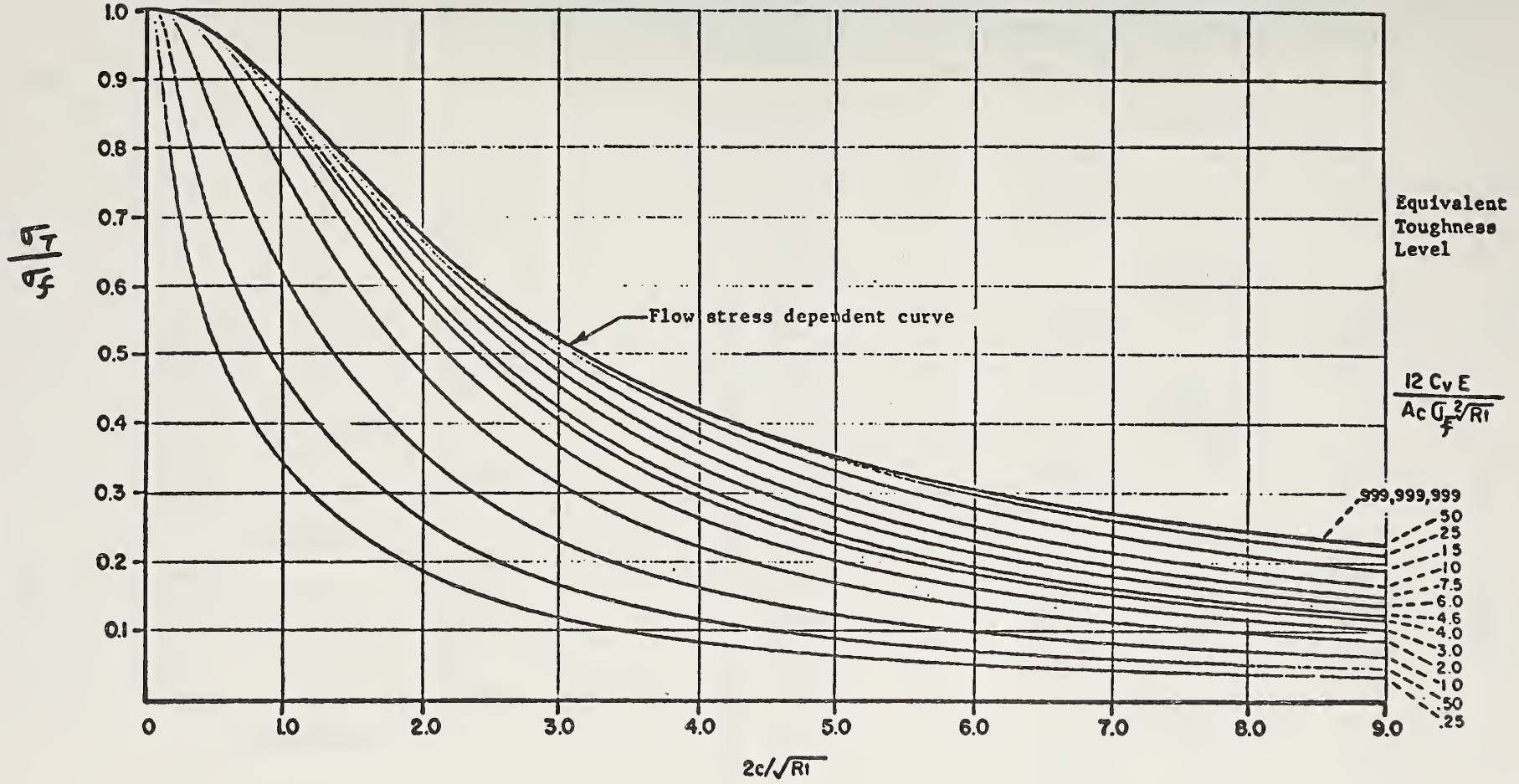

Figure 27. Through wall flaw size-toughness relationship for cylindrical pressure vessels. (Diagram courtesy of W. Maxey of Battelle Memorial Institute, Columbus, Ohio.)

METRIC CONVERSION FACTORS

Approximate Conversions to Metric Measures

Symbol	When You Know	Multiply by	To Find	Symbol
	LENGTH			
in	inches	*2.5	centimeters	cm
ft	feet	30	centimeters	cm
yd	yards	0.9	meters	m
mi	miles	1.6	kilometers	km
	AREA			
in^2	square inches	6.5	square centimeters	cm^2
ft^2	square feet	0.09	square meters	m^2
yd^2	square yards	0.8	square meters	m^2
mi^2	square miles	2.6	square kilometers	km^2
	acres	0.4	hectares	ha
	MASS (weight)			
oz	ounces	28	grams	g
lb	pounds	0.45	kilograms	kg
	short tons (2000 lb)	0.9	tonnes	t
	VOLUME			
tsp	teaspoons	5	milliliters	ml
Tbsp	tablespoons	15	milliliters	ml
fl oz	fluid ounces	30	milliliters	ml
c	cups	0.24	liters	l
pt	pints	0.47	liters	l
qt	quarts	0.95	liters	l
gal	gallons	3.8	liters	l
ft^3	cubic feet	0.03	cubic meters	m^3
yd^3	cubic yards	0.76	cubic meters	m^3
	TEMPERATURE (exact)			
°F	Fahrenheit temperature	5/9 (after subtracting 32)	Celsius temperature	°C

*1 in = 2.54 (exactly). For other exact conversions and more detailed tables, see NBS Misc. Publ. 286, Units of Weights and Measures, Price $2.25, SD Catalog No. C13.10:286.

Approximate Conversions from Metric Measures

Symbol	When You Know	Multiply by	To Find	Symbol
	LENGTH			
mm	millimeters	0.04	inches	in
cm	centimeters	0.4	inches	in
m	meters	3.3	feet	ft
m	meters	1.1	yards	yd
km	kilometers	0.6	miles	mi
	AREA			
cm^2	square centimeters	0.16	square inches	in^2
m^2	square meters	1.2	square yards	yd^2
km^2	square kilometers	0.4	square miles	mi^2
ha	hectares (10,000 m^2)	2.5	acres	
	MASS (weight)			
g	grams	0.035	ounces	oz
kg	kilograms	2.2	pounds	lb
t	tonnes (1000 kg)	1.1	short tons	
	VOLUME			
ml	milliliters	0.03	fluid ounces	fl oz
l	liters	2.1	pints	pt
l	liters	1.06	quarts	qt
l	liters	0.26	gallons	gal
m^3	cubic meters	35	cubic feet	ft^3
m^3	cubic meters	1.3	cubic yards	yd^3
	TEMPERATURE (exact)			
°C	Celsius temperature	9/5 (then add 32)	Fahrenheit temperature	°F